이학박사학위논문

북반구 겨울철의 Maritime Continent 상에서의 계절내 진동과 일변동성 간의 상호작용

Scale Interaction between MJO and the Diurnal Variability over the Maritime Continent during Austral Summer

2012년 8월

서울대학교 대학원

지구환경과학부

오 지 현

ABSTRACT

Scale Interaction between MJO and the Diurnal Variability over the Maritime Continent during Austral Summer

Ji-Hyun Oh
School of Earth and Environmental Sciences
The Graduate School
Seoul National University

This study aims to investigate the scale interaction between the diurnal variability and MJO over the Maritime Continent during Austral summer.

As the first part for this study, the impact of MJO on the diurnal cycle of rainfall over the western MaritimeContinent during the Austral summeris examined. For this purpose, Cyclostationary Empirical Orthogonal Function (CSEOF) analysis is applied to the Tropical Rainfall Measuring Mission (TRMM) rain rate and the Japanese Reanalysis Analysis-25 (JRA-25) data for the period of 1998-2008. Real-time Multivariate MJO (RMM) index by Wheeler and Hendon (2004) is adopted to define the intensity and the phase of MJO. It is demonstrated that hourly maximum rain rate over the domain tends to increase when convectively active phase of MJO approaches the

Maritime Continent. In contrast, hourly maximum rain rate tends to decrease when convectively suppressed phase of MJO resides over the region. The rain rate change due to MJO over the ocean is quite different from that over land. During the mature stage of MJO over the Maritime Continent, diurnally varying rain rates over the ocean indicate maximum values while terrestrial rain rates show minimum values throughout the day. Thus, precipitation becomes more intense in the morning over the Java Sea and is weakened in the evening over Borneo and Sumatra during the mature stage of MJO. During the decaying stage of MJO over the Maritime Continent, the diurnal cycle of precipitation weakens significantly over the ocean but less than over the land.

Analyses suggest that the anomalous lower level winds accompanied by MJO interact with the monsoonal flow over the Maritime Continent. Westerlies induced by MJO convection in the mature stage are superimposed on the monsoonal westerlies over the equator and increase wind speed mainly over the Java Sea due to the blocking effect of orography. Mountainous islands induce flow bifurcation,causing near-surface winds to

converge mainly over the oceanic channels between two islands. As a result, heat flux release from the ocean to the atmosphere is enhanced by the increased surface wind resulting in instability as described in the wind-induced surface heat exchange (WISHE) mechanism. This may contribute to heavy rainfall over the Java Sea in the morning during the mature stage. On the other hand, convergence and vertical velocity over the islands, which play important roles in inducing nighttime rainfall, tend to be weak in the evening during the mature stage of MJO. Strong westerlies arising from MJO and the seasonal flow during the mature stage tend to interrupt convergence over islands. This interruption of convergence by MJO gives rise to decreased rain rates over the land regions.

As the second part of the study, modeling experiments are conductedto investigate the impact of the diurnal cycle on MJO during the Australian summer.Physical initialization and a nudging technique enable usto assimilate the observed TRMM rain rate and atmospheric variables from the National Centers for Environmental Prediction–National Center for Atmospheric Research Reanalysis 2 (R2) into the Florida State University

Global Spectral Model (FSUGSM), resulting in a realistic simulation of the MJO. Model precipitation is also significantly improved by TRMM rain rate observation viathe physical initialization.We assess the influence of the diurnal cycle on the MJO by modifying the diurnal component during the model integration. Model variables are nudged toward the daily averaged values from R2. Globally suppressing the diurnal cycle (NO_DIURNAL) exerts a strong impact on the Maritime Continent. The mean state of precipitation increases and intraseasonal variability becomes stronger over the region. It is well known that MJO weakens as it passes over the Maritime Continent.However, the MJO maintains its strength in the NO_DIURNAL experiment, and the diminution of diurnal signals during the integration does not change the propagating speed of the MJO.Diminishing the diurnal cycle in NO_DIURNAL seems to consume less moist static energy (MSE), which is required to trigger both diurnal and intraseasonal convection. Thus, the remaining MSE may play a major role along with larger convective instability and stronger lower level moisture convergence in intensifying the MJO over the Maritime Continent in the

model simulation.

Key words: MJO, Diurnal cycle, Scale interaction, Physical initialization, Maritime Continent

Student Number: 2007-30103

Contents

List of Figures

List of tables

Chapter 1

Introduction

1.1. Backgrounds

The Maritime Continent, consists of islands and seas off Southeast Asia, is a major atmospheric heat source that plays an essential role in the earth's climate system (Ichikawa and Yasunari 2005). Many islands in the Maritime Continent are mountainous and complex land/ocean geography (Figure 1.1). The complex terrain of islands and seas in this region gives rise to strong local variations of the rainfall annual cycle and diurnal cycles. The Maritime Continent has the conspicuous diurnal variation of rainfall (Ichikawa and Yasunari 2006), which exhibits a distinct land-sea contrast (Ichikawa and Yasunari 2006; Qian 2008). While a maximum amount of rainfall occurs in the late afternoon/evening over land, precipitation over the oceanic region

reaches a maximum at night/early morning (Yang and Slingo 2001; Ichikawa and Yasunari 2006; Zhou and Wang 2006; Qian 2008). In addition, the diurnal variation over the Maritime Continent interacts with the longer-term weather and climate variations, such as MJO, monsoon surges, intraseasonal oscillation, and ENSO (Chang et al 2004a).The multi-scale interaction between the diurnal cycle in the Maritime Continent and large-scale processes has an important implication for global atmospheric general circulation because of the geographical location of the Maritime Continent (Qian 2008).

Since Madden-Julian Oscillations (MJOs) with periodicities of ~30-60 days were observed in various meteorological variables, numerous observational and modeling studies have been conducted in regard to their initiation, propagation, general characteristics (Rui and Wang 1990; Hendon and Salby 1994; Slingo et al. 1996; Sperber 2003).According to Rui and Wang (1990), the zonal coverage of an MJO event is roughly 12,000-20,000 km. The typical MJO shows large-scale wind structure which is described in terms of equatorial waves coupled to deep convection. The low-level easterlies and

upper level westerlies which exist to the east of the convective center are referred as Kelvin wave types, and the low-level westerlies (upper level easterlies) and associated pair of cyclonic circulation straddling the equator are the features of the equatorial Rossby wave (Rui and Wang 1990). The spectral peak is at zonal wave number 1 for the zonal wind associated with MJO in general (see Figure 3 of Zhang 2005). Austral summer MJO develops over the Indian Ocean and propagates eastward along the equator passing over the Maritime Continent. Earlier studies revealed that MJO is also closely tied with atmospheric phenomena on various temporal and spatial scales such as Asian/Australian monsoons (Sui and Lau 1992; Lawrence and Webster 2002; Hendon and Liebmann 1990), tropical cyclones (Maloney and Hartmann 2000; Hall et al. 2001) and ENSO (Kessler and Kleeman 2000; Zhang and Gottschalck 2002).

According to previous studies, the Maritime Continent tends to weaken MJO convection (Seo and Kim 2003; Hsu and Lee 2005; Wu and Hsu 2009). A convectively active phase of MJO was observed to shift suddenly from one region to another over the Maritime Continent (Ichikawa and Yasunari

2007). After its steady propagation is disturbed by the Maritime Continent, MJO rejuvenates and keeps on moving eastward in austral summer. Inness and Slingo (2006) mentioned the enhanced diurnal cycle of convection around Maritime Continent affects the development of MJO by dissipating moist static energy on a fast time-scale resulting in the interference of the slow build-up and release of energy associated with MJO.

The scale interaction is defined as the process that describes the influence of the large-scale and low-frequency variability on small spatial scale high-frequency variability of the climate system and vice versa (Slingo et al. 2003). In this study, we examine the scale interaction between the diurnal cycle and MJO over the Maritime Continent during Austral summer.

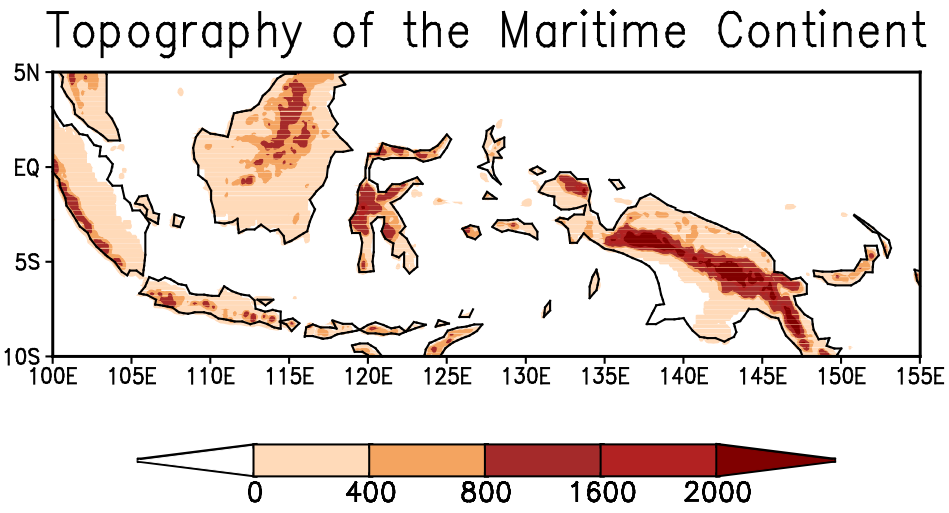

Figure 1.1 Terrain height (m) in the Maritime Continent.

1.2.Motivations and Objectives

Although the importance of scale interactions on diurnal, intraseasonal, and seasonal timescales for the mean and variability of the climate system has been emphasized (Slingo et al., 2003; Qian et al., 2010), relatively less attention has been paid to the scale interaction between the diurnal cycle and MJO especially over the Maritime Continent. Furthermore, Most of the studies on the scale interaction between the diurnal cycle and the MJO have mainly focused on the modulation of the diurnal cycle by the MJO rather than the influence of the diurnal cycle on the MJO. For example, Ichikawa and Yasunari (2006, 2008) showed that the diurnal cycles of rainfall over Borneo and New Guinea, major islands of the Maritime Continent, are modulated by the low level winds varying on intraseasonal time scales using TRMM precipitation radar data. Tian et al. (2006) demonstrated that the amplitude of diurnal cycle of tropical deep convective cloud (DCC) amount is enhanced (reduced) over both land and the ocean during the convectively enhanced (suppressed) phase of the MJO while the diurnal phase of DCC is rarely changed by MJO. Rauniyar and Walsh (2011) investigated the

characteristics of the diurnal cycle of rainfall during different phases of the MJO over the Maritime Continent. They showed the diurnal cycle depends on the phase of the MJO, especially over the oceanic regions.

Understanding roles of multi-scale interaction of the regional climate is crucial not only for the regional climate predictability but also the global climate sensitivity and predictability. This study aims to investigate the two-way scale interaction between the diurnal variability and MJO over the Maritime Continent during Austral summer. Austral summer period, during which MJO signals are strongest, is chosen in the present study.

As the first part of this study, we examine the impact of MJO on the diurnal cycle of rainfall over the western Maritime Continent consisting of Borneo, the Malay Peninsula, Sumatra, and Indonesian islands during Austral summer. In particular, the MJO modulation of the diurnal variation of rainfall over the Maritime Continent with specific distinction of the terrestrial and the oceanic regions is mainly focused. In addition, plausible physical explanations for the MJO modulation of the diurnal cycle are

offered. Statistical analysis called the cyclostationary empirical orthogonal function (CSEOF) technique is used. This method enables us to extract the diurnal cycle from the datasets as well as the temporal variation of its strength.

As the second part of the study, we investigate the influence of the diurnal cycle on MJO over the Maritime Continent during Austral summer by using Florida State University Global Spectral Model (FSUGSM). A continuous nudging, which is one of the assimilation technique, is adopted for the model experiment. We assess the performance of the model with respect to the mean climate and intraseasonal oscillation. As current numerous GCMs have been problematic in representing the MJO, it is one of important challenges to simulate MJO more realistically, as well (Slingo et al 1996). We neglect diurnal cycle in the model simulation by applying the assimilation technique to examine the impact of the diurnal cycle on MJO simulation. Even quite small but systematic changes to the diurnal cycle can rectify mean climate, we investigate the representation of the seasonal cycle and MJO in the simulation without diurnal variability.

1.3. Data and Method

1.3.1 Data

TRMM 3B42 (version 6) rainfall data, which are derived from a combination of high-quality microwave estimates and variable rain rate infrared (IR) estimates, are used for the present study (http://trmm.gsfc.nasa.gov/3b42.html). The data are intended to be used to take advantage of the fine scales to create averages appropriate to the user's application (Huffman et al. 2007). The TRMM Multi satellite precipitation Analysis (TMPA) is derived by using an optimal combination of TRMM and other passive microwave precipitation estimates from instruments on-board different low-Earth-orbit satellites. The merged microwave product is calibrated with infrared (IR) estimates from the rapid time capability of geostationary-Earth-orbit satellites as complementary estimates to those from the microwave measurements. The IR radiometer has the advantage of providing estimates with high spatial resolution and very good time sampling. However, the IR radiometer measures the brightness temperature at the top of the cloud, which is an indirect rainfall measuring method. In

this regard, rain gauge analyses are also adopted for better estimates (Huffman et al. 2007). Acquired via anonymous ftp from disc2.nascom.nasa.gov, the dataset covers 50°S to 50°N with a 0.25° longitude–latitude spatial resolution at a 3-hr time interval.

In order to explain the physical and dynamical processes associated with the diurnal cycle of precipitation over the western Maritime Continent during the austral summer (DJF) and the impact of MJO on the diurnal variation, Japanese 25-yr Reanalysis (JRA-25) provided by the Japan Meteorological Agency and the Central Research Institute of Electric Power Industry (JMA-CRIEPI) were also used. The JRA-25 dataset has a 1.25°×1.25°horizontal resolution and a 6-hr temporal resolution and was acquired from the web site http://jra.kishou.go.jp/JRA-25 (Onogi et al. 2007).

The National Centers for Environmental Prediction/National Center for Atmospheric Research Reanalysis 2 (NCEP/NCAR R2, hereafter R2) data are provided by the NOAA/OAR/ESRL PSD, Boulder, Colorado, USA,

from their Web site at http://www.cdc.noaa.gov/. Wind, temperature, humidity and surface pressure are adopted from the dataset for analysis nudging and model initialization in modeling.

In addition, daily-averaged outgoing long wave radiation (OLR) data from the National Oceanic and Atmospheric Administration (NOAA) were used to extract the patterns of eastward propagating MJO. The Real-Time Multivariate MJO (RMM) index derived by Wheeler and Hendon (2004) was acquired from the website of the Bureau of Meteorology Research Centre, Australia (http://www.cawcr.gov.au/bmrc/).

To verify the quality of precipitation simulated by each modeling experiment, daily precipitation from the GPCP 1-degree Daily dataset (GPCP 1DD; GPCP) is employed (Huffman et al. 1997).

1.3.2 CSEOF analysis

Empirical orthogonal function (EOF) analysis was first performed on the TRMM rain rate. Then, CSEOF analysis was conducted in the EOF space with a nested period of 1 day (=eight 3-hour intervals) in order to extract the

diurnal cycle of the rain rate. The first 100 EOFs were used as basis functions; the 100 EOFs together explain about 50% of the total variability.

In CSEOF analysis (Kim et al. 1996; Kim and North 1997), space-time data $T(r,t)$ are decomposed into

$$T(r,t)=\sum_n LV_n(r,t)PC_n(t), \quad (1)$$

where $LV_n(r,t)$ are cyclostationary loading vectors and $PC_n(t)$ are corresponding principal component time series. The cyclostationary loading vectors are periodic in time

$$LV_n(r,t)=LV_n(r,t+d), \quad (2)$$

where d is the nested period. Thus, each $LV_n(r,t)$ describes daily and sub-daily physical evolution of rain rate and corresponding PC time series, $PC_n(t)$, describes the variation of the amplitude on time scales longer than a day. CSEOF loading vectors, $LV_n(r,t)$, are time dependent and periodic because they are derived from a time-dependent and periodic covariance function. In order to examine the MJO's modulation of the diurnal cycle, the CSEOF analysis is applied to the datasets described above for the 10 austral

summers (DJF) from 1998/99 to 2007/08. Each winter consists of 90 days.The domain of analysis for the study is 100°E-125°E×10°S-5°N; this region covers the western part of the Maritime Continent, which encounters eastward propagating MJOs

1.3.3 Regression analysis

After CSEOF analysis is performed separately for individual variables, regression analysis should be conducted in order to make individual variables physically consistent with each other (Seo and Kim 2003). The PC time series of a predictor variable, such as wind, are regressed on the PC time series of precipitation (target variable in this study):

$$PC_n(t) = \sum_{m=1}^{M} \alpha_m^{(n)} PCP_m(t) + \varepsilon^{(n)}(t), \qquad n = 1,2,3,... \tag{3}$$

where $PC_n(t)$ are the PC time series of the rain rate, $PCP_m(t)$ are the PC time series of a predictor variable, and $\alpha_m^{(n)}$ are regression coefficients. Then, a new loading vector is obtained by

$$LVP_n^{(reg)}(r,t) = \sum_{m=1}^{M} \alpha_m^{(n)} LVP_m(r,t), \tag{4}$$

where $LVP_m(r,t)$ are the loading vectors of the predictor variable and

$LVP_n^{(reg)}(r,t)$ denotes the new loading vector of the predictor variable, which is physically consistent with the nth loading vector of the rain rate. As a result of the regression analysis, the entire data can be written as

$$Data(r,t) = \sum_n \{PR_n(r,t), ST_n(r,t), U_n(r,t), V_n(r,t), ...\} PC_n(t), \qquad (5)$$

where $PR_n(r,t)$ represents the loading vectors of the rain rate (target variable) and $ST_n(r,t)$, $U_n(r,t)$, $V_n(r,t)$, for example, are the regressed loading vectors of surface air temperature, zonal wind, and meridional wind. Although the physical evolutions of individual variables are distinct, their amplitudes are all governed by one time series, $PC_n(t)$, which is the PC time series of the rain rate (target variable).

1.3.4 Classification of MJO

To investigate the scale interactionbetween MJO on the diurnal cycle of rainfall over the Maritime Continent, it is necessary to define the dates in which the convection of MJO reaches the Maritime Continent. These dates were determined by using the Real-Time Multivariate MJO (RMM) index derived by Wheeler and Hendon (2004). The RMM index is constructed by

the two leading principal component time series, RMM1 and RMM2, of the EOFs of zonal winds at 850 hPa and 200 hPa. The RMM1 and RMM2 construct the two-dimensional phase space of MJO and represent the location of MJO in the phase space as a point (RMM1, RMM2).Distance of a point from the origin determines the amplitude of MJO. The phase space is divided into 8 sectors, from which the location of MJO convection center between Africa and the eastern Pacific can be inferred. We utilized the RMM index for composite analysis. Only the cases with the amplitude of MJO being greater than unity were chosen.

1.3.5 FSUGSM

The FSUGSM, which is an atmospheric general circulation model with 27 sigma vertical levels and a horizontal resolution of T63,is used. Detailed model configuration and selected FSU physics package in this study are described by Cocke and Larow (2000). Using the FSUGSM as a basic modeling system, we adopt the continuous assimilation system by implementing analysis nudging for the model dynamic equation set and a rain rate nudging procedure for the convective parameterization component

(in this study, modified Kuo scheme; See Krishnamurti et al. 1983 for details) of the model. The procedure for assimilation of rain rate is based on the method described by Nune and Cocke (2004). The assimilation technique we use relies largely on a physical initialization (PI) method (Krishnamurti et al. 1991, 1994) that primarily includes rain rate nudging toward observed rain rates as well as Newtonian nudging of prognostic model variables (horizontal winds, temperature, specific humidity, and surface pressure) toward reanalysis. The Newtonian nudging, which keeps the model variables similar to the variables in the original reanalysis, is applied by including an additional nudging term in the tendency equation. The Newtonian nudging can be mathematically expressed as

$$\dot{X} = F(X) + \alpha(X - X_a) \qquad (6)$$

In this expression, F is the nonlinear model equation, α is the nudging coefficient, X is the model state variable, and X_a is the variable from reanalysis. Since reanalysis is provided every six hours, X_a during the six-hour interval is linearly interpolated.

The model is also nudged toward the observed rain rates by modifying a specific humidity column. The PI technique enables the assimilation of TRMM rain rate into the FSUGSM using a reverse cumulus algorithm. The reverse algorithm generates constraints to restructure the distribution of moisture fields produced by the FSUGSM. Through the rainfall nudging, the humidity vertical profile experiences modifications as a function of the observed and predicted rain rates. As a result, model precipitation is brought closer to the observed rain rate. A vertical structure function (Nune and Cocke 2004) is used for the modified moisture.

$$q_m = \frac{R_o}{R_p} q + \frac{(1/g)\int_{\sigma_t}^{\sigma_b} q\, d\sigma}{(1/g)\int_{\sigma_t}^{\sigma_b} d\sigma} \left(1 - \frac{R_o}{R_p}\right) \qquad (7)$$

Here, q_m is the modified specific humidity, q is the specific humidity before PI, R_o and R_p are the observed and predicted rainfall rates and σ_b and σ_t denote the σ levels at the base and top of the clouds, respectively. However, the Kuo scheme, which constrains the regions where model rain rates are modified, requires convective instability and moisture convergence for the initialization. The modification is applied at every time step, but it is

limited to 10% for any one time step to prevent abrupt drift of the model state variables. The rain rate nudging is not conducted unless the model produced or observed rain rates exceed 10 mm/day. Details of this procedure are described by Nune and Cocke (2004).

During the integration, the optimum interpolation sea surface temperature (OISST) is used as a lower SST boundary condition and is updated weekly. Land surface conditions such as vegetation and snow depth are prescribed by their monthly climatology.

1.3.5 Experimental design

To examine the impact of the diurnal cycle on the MJO, we design two simulations that are identical in all aspects except the following. One simulation includes nudging of rain rate that varies at three-hour intervals and Newtonian nudging of dynamic variables from NCEP R2at six-hour intervals (hereafter CTRL). The other simulation incorporates nudging of daily averaged TRMM rain rate and daily averaged prognostic variables from NCEP R2, applying the same nudging coefficients used in

CTRL(hereafter NO_DIURNAL). To diminish the variability of the diurnal cyclein the NO_DIURNAL experiment, the daily averaged values of rain rate and relevant model variables described above are nudged every three hours and every six hours, respectively, in a form of incremental analysis update to prevent assimilation hock (Bloom et al.1996). The diurnal cycle is not completely removed from the NO_DIURNAL because there is still diurnally varying radiation in both simulations. However, the applied Newtonian relaxation toward incorporated analysis acts as a constraint to accommodate corresponding heating associated with the assimilated convection. The rain rate nudging is conductedin an area extending from 50° S to 50° N; the dynamic nudging is conducted over the whole globe. The outputs from CTRL and NO_DIURNAL are examined for four austral summers (DJF), when the MJO is at maximum amplitude, from 2000/01 to 2003/04. In addition, the NO_NUDGING experiment, in which the rain rate nudging and Newtonian nudging are turned off, is also performed to evaluate the performance of the assimilation technique in FSUGSM.

Chapter 2

Diagnostics of the Impact of MJO on the Diurnal Cycle of Rainfall over the Maritime Continent during Austral Summer

After the launch of the TRMM satellite in 1998, various data acquired from the mission were analyzed in an attempt to understand the diurnal cycle over the tropics (Nesbitt and Zipser 2003; Bowman et al. 2005; Yang and Smith 2006; Zhou and Wang 2006; Ichikawa and Yasunari 2007). These studies showed that the diurnal cycle of rainfall over the terrestrial region differs significantly in phase and mechanismfrom that of the oceanic region (Nesbitt and Zipser 2003;Bowman et al. 2005).It was also noted that the relationship between the diurnal variation of rainfall and large-scale disturbance associated with MJO over the ocean differs from that over land (Ichikawa and Yasunari 2007). Yet, little is known about the disparate impact of MJO on the diurnal cycle over the terrestrial and the oceanic regions of the Maritime Continent.Due to the land-sea contrast of latent heat

flux and the orographic effect over land, there exist distinctinteractions between the diurnal cycle of precipitation and MJO over land and over the ocean.

Although previous studies have been conducted using various analysis technique and data to reveal the impact of the MJO on the diurnal cycle over the Maritime Continent, they are not in agreement yet. This study focuses on this issue, particularlyon the MJO's modulation ofthe diurnal variation of rainfall over the Maritime Continent with specific distinction of the terrestrial and the oceanic regions. In addition, plausible physical explanations for the MJO's modulation of the diurnal cycle are offered.

2.1.Characteristics of the climatological diurnal cycle over the western Maritime Continent

The first CSEOF of the TRMM rain rate represents the diurnal cycle of precipitation in the austral summer (DJF) over the western Maritime Continent. The diurnal variation of precipitation and other physical variables

are shown in Figure 2.1. As already mentioned in previous studies, there exists a distinct land-ocean contrast in the phase of the diurnal cycle of rainfall (Yang and Slingo 2001; Ichikawa and Yasunari 2006; Mori et al. 2004). Rainfall over the islands is maximum in late afternoon/evening and minimum in early morning. Panels (a)-(h) of Figure 2.1 exhibit that rainfall begins along the coastline and gradually shifts inland (Borneo and Sumatra) during 1700-2300 LST. After reaching its maximum over the islands, rainfall shifts offshore during 0200-1100 LST.

Other Evolution of other atmospheric variables associated with the diurnal cycle of rainfall is shown in Figures2.1(i)-(p). Since the land surface has a lower heat capacity,temperature variation by solar heating is more significant over land than over the ocean. When the sun rises, temperature over land increases rapidly until the sun reaches its maximum altitude. This causes the pressure gradient to increase between land and ocean and static destabilization of the atmosphere over land (Bowman et al. 2005; Yang and Smith 2006). Daytime sea breeze is induced due to the pressure gradient, resulting in moisture supply by sea breeze together with a forced ascent of

air. Equivalent potential temperature difference between 850 hPa and 500hPaindicates conditional instability. The convective instability is enhanced over the islands at 1400 LST. Strong upward motion and lower level convergence prevails over islands, such as Borneo, Sumatra, and Sulawesi at 2000 LST. As a result, late-afternoon and evening precipitations tend to develop over land. The situation reverses after the sunset. Radiative cooling during the night stabilizes the atmospheric column over land and precipitation gradually diminishes until morning.

According to Qian (2008), since mountain-valley breezes are roughly in phase with land-sea breezes over the mountainous coastal region, those may combine to strengthen the diurnal cycle of winds and form extended land-sea breezes. On the other hand, low-level convergence of the prevailing northeasterly monsoonal flow and the land breeze contributes to oceanic precipitation adjacent to the northwest Borneo from midnight till morning (Houze et al. 1981; Ichikawa and Yasunari 2006; Liberti et al. 2001). Similarly, land breezes from adjacent islands converge over the seas between the islands (e.g. between Borneo and southern Sumatra) at night

and induce nighttime precipitation (Qian 2008).

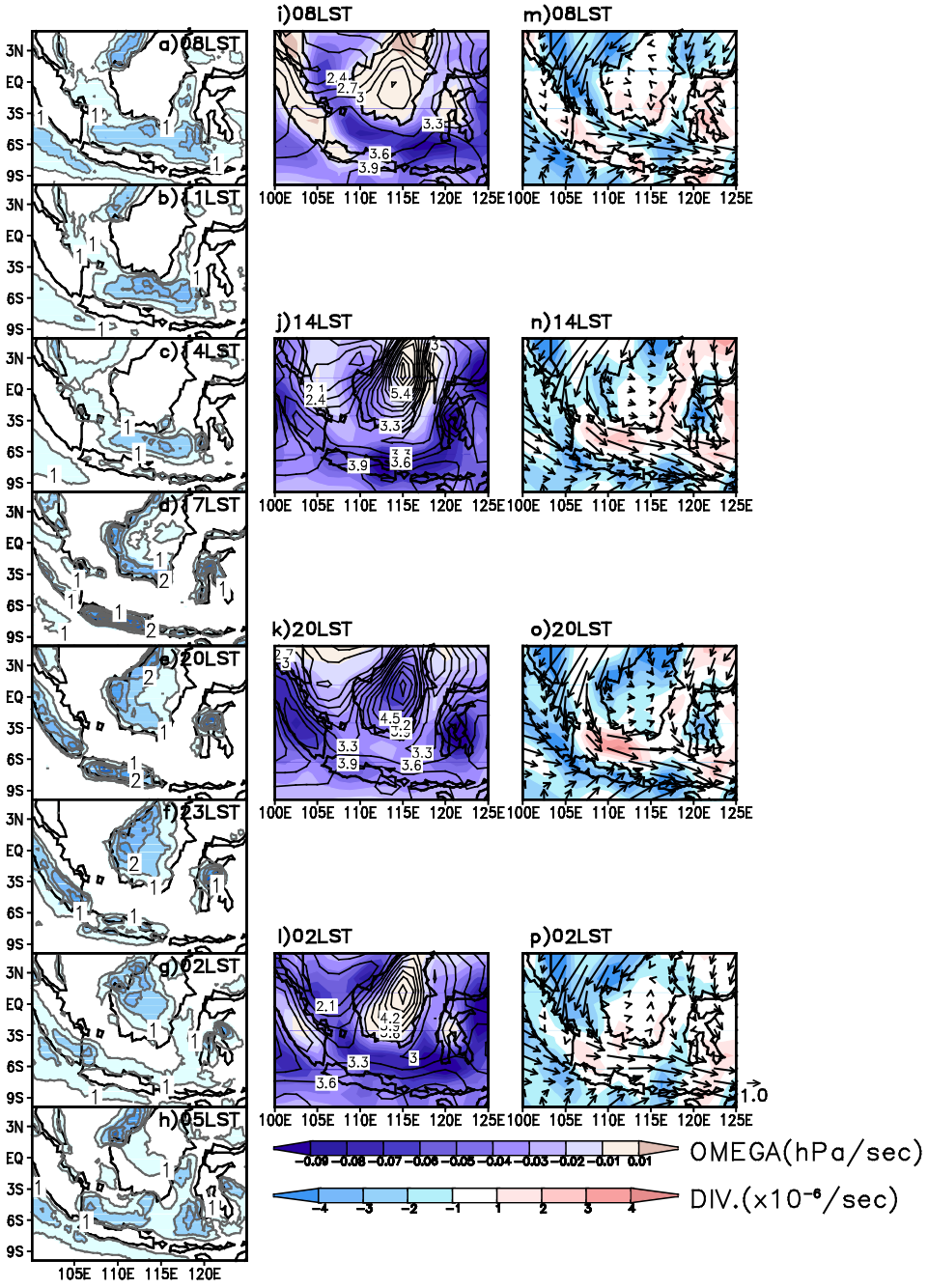

Figure 2.1 Evolution of (a-h) TRMM rain rate (mm hr-1), (i-l) 500 hPa pressure velocity (shaded, hPa sec-1) and difference of equivalent potential temperatures between 850 hPa and 500 hPa (contoured, K), and (m-p) 10 m

wind (vector, m sec-1) and surface divergence (shaded, sec^{-1}) in association with the diurnal cycle.

2.2. Spatial distribution of MJO

Composite maps of daily OLR and 850 hPa wind anomalies for individual phases of MJO based on the RMM index are shown in Figure 2.2. For composite analysis, only cases in which the amplitude of MJO was greater than unity were chosen; the number of days selected for compositing is given in parentheses for each phase in Figure 2.2. The rectangular box in the composite domain denotes the western Maritime Continent. As shown in the figure, eastward propagating MJO are reasonably well captured with respect to the RMM index. MJO convection initiated over the western Indian Ocean in phase 1 moves eastward and approaches the western part of the Maritime Continent near Sumatra, Borneo and the Java Sea in phase 3 (see also Seo and Kim 2003). Prevailing easterly wind anomalies in phase 1 change into westerly wind anomalies in the western regime of the convective area in phase 2. During phases 3-5, convectively enhanced MJO phase passes over the Maritime Continent. Westerly wind anomalies are dominant in the analysis domain. In phases 6-8, suppressed convection penetrates the Maritime Continent followed by easterly wind anomalies.

These DJF composite patterns based on the RMM index show similar evolutionary features of MJO as shown in previous studies (e.g., Wheeler and Hendon 2004).

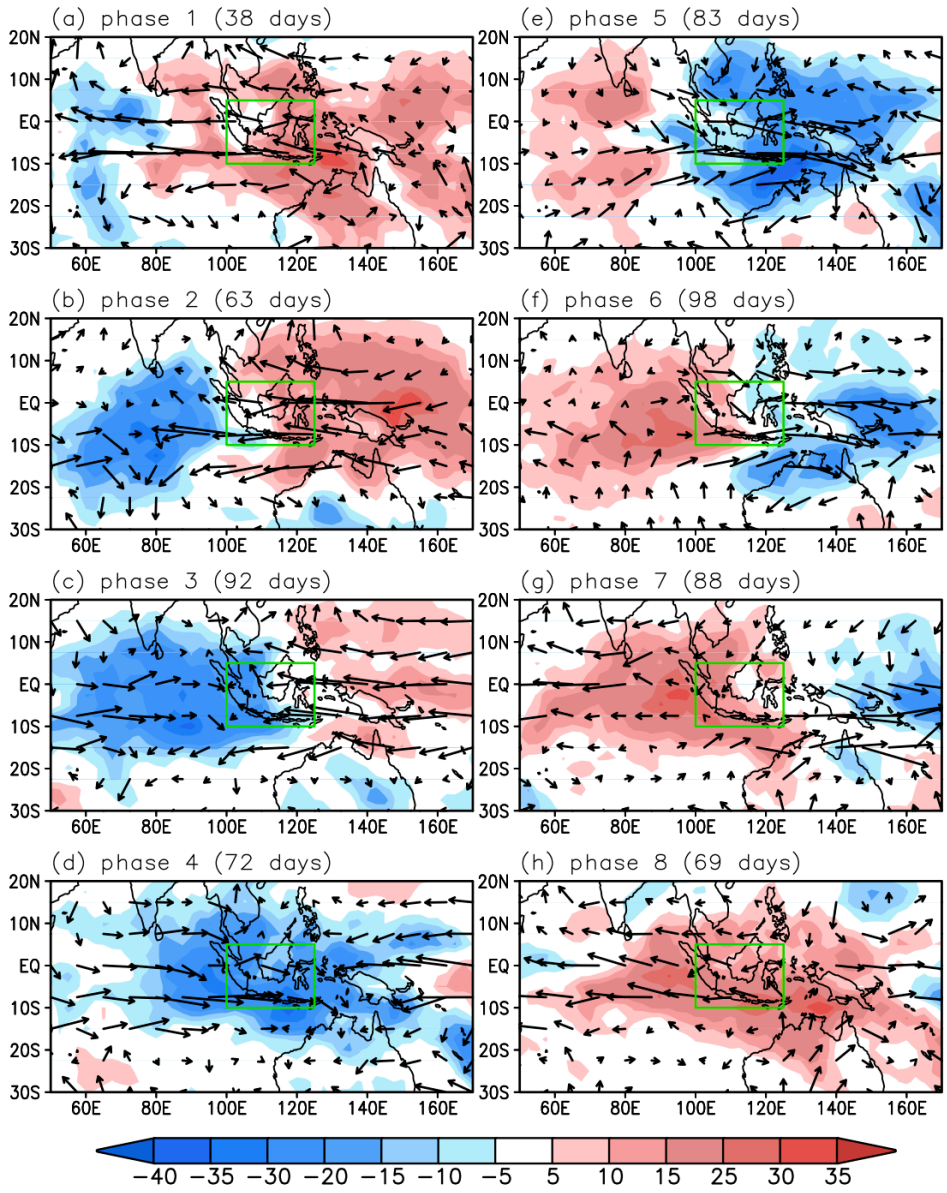

Figure 2.2 Composite of OLR and 850 hPa wind anomalies for individual phases of MJO based on the RMM index. A rectangular box in each panel denotes the analysis domain for the present study. The number in parentheses denotes the number of days for each phase withthe MJO amplitude greater than unity during the 10 austral summer (DJF) years (97/98-07/08).

2.3 Influence of MJO on the diurnal variation of rainfall

Figure 2.3 (a) shows the PC time series of the 1st CSEOF of the TRMM rain rate, of which the loading vector was shown in Figure2.1. The mean value of the PC time series is 1.14 and its standard deviation is 1.26 exhibiting significant fluctuations of the diurnal cycle of precipitation over the study domain. The PC time series shows the modulation of the diurnal cycle of precipitation on time scales longer than 1 day; one possible source of modulation may be MJO over the western Maritime Continent. The PC time series exhibits significant power for the period of ~60 days, which is known as the periodicity of MJO (Figure 2.4). This suggests that MJO exerts considerable influence on the diurnal variation of precipitation over the Maritime Continent. In order to examine the impact of MJO, the mean and the standard deviation of the PC time series were calculated as a function of the phase of MJO and are shown in Figure2.3(b). The average amplitude of the seasonal cycle is at its maximum during phase 3 and at its minimum during phase 6, respectively. As shown in Figure2.2, active convection develops in phase 3 and persists until phase 5 over the Maritime Continent.

In contrast, convection is suppressed over the domain during phases 6 and 7. Figure2.3(b) suggests that the diurnal cycle of precipitation is enhanced during the active phases and is reduced during the inactive (suppressed) phases of MJO.

Among the eight MJO phases categorized by the RMM index, three phases (3, 5, and 7) of the MJO are chosen to examine the physical process pertaining to the interaction between MJO and the diurnal cycle of precipitation over the western Maritime Continent. Phase 3 is considered to be not only transition stage of convective MJO from the Indian Ocean to the western Maritime Continent also a developing stage of convection over the western Maritime Continent, and phase 5 is a mature stage of MJO in which fully developed and expanded convection is located over the Maritime Continent. On the other hand, phase 7 represents the decaying stage of convection. The domain averaged loading vector of the first CSEOF (diurnal cycle) of the rain rate for phases 3, 5, and 7 of MJO and the climatological diurnal cycle are shown in Figure 2.5(a). The diurnal cycle for each phase of MJO in Figure 5 is scaled by multiplying the square root

of the respective eigenvalue so that the magnitude of the diurnal cycle can be compared between the different phases of MJO.

The climatological diurnal cycle of the domain averaged rain rate exhibits bimodal peaks—the morning peak is associated with an increase of the rain rate over the ocean and the evening peak is related to an increase of the rain rate over land. Consistent with Figure 2.3(b), the diurnal cycle during the MJO phase 3 has a greater rain rate than the climatological diurnal cycle. The magnitude of the diurnal cycle during phase 5is larger in the morning than the climatology, however, it is smaller in the evening. The rain rate decreases markedly in phase 7.

The diurnal cycle of the rain rate for the oceanic and land areas were also computed separately. Land areas and ocean areas clearly exhibit distinct diurnal cycles of rain rate as already discussed above (Figures 2.5(b) and (c)); maximum rain rate occurs in the evening (2000 LST) over land regardless of the phase of the MJO whereas maximum occurs in the morning (0500 LST or 0800 LST) over the oceans. The diurnal cycle of

precipitation over the seas has a smaller range compared to that over the islands.

As shown in Figure2.5(a) and discussedabove, the oceanic diurnal cycle is enhanced during the active phase (phases 3 and 5) of MJO and is suppressed during the inactive phase (phase 7). Not only the magnitude but also the phase of the diurnal cycle is slightly altered with respect to the phase of MJO. Duringconvectively active phases (phases3 and 5) of MJO, the overall magnitude of the rain rate increases throughout the day with a peak rain rate at 0500 LST. In inactive phase (phase 7), in contrast, the rain rate reduces considerably and a peak appears at 0800 LST—about 3 hours later than the active phases.Since TRMM has a 3-hr temporal resolution, however, it is inconclusive that the decaying phase of MJO induces a 3-hr delay of rainfall peaks over the ocean. Further, rain rates at 0500 LST and 0800 LST are not significantly different. It is difficult to establish that the delay of the rainfall peak is statistically and physically significant.

On the other hand, the impact of MJO appears to be quitedifferent over land

withan increased diurnal cycle during the transition (developing) stage and a decrease diurnal cycle during the mature stage.Contrary to the oceanic case, the rain rate of the diurnal cycle records minimum values throughout the day in phase 5. During the decaying stage of MJO, the magnitude of the diurnal cycle over land is also reduced but the peak time (2000 LST) does not change.

Figure 2.6(a) shows the percentage of the oceanic region recording maximum rain rates at each local time based on the entire record. The distribution pattern is similar to the diurnal cycle of rain rate over the ocean (Figure 2.5(c)). This is an expected result since hourly rain rate tends to increase with increase of precipitation. However, this figure denotes the regional intensity of the rain rate in each time step rather than overall rainfall amount. According to climatology, maximum rain rates are most widely observed, over 25% of the study domain, at 0800 LST. In contrast, maximum rates are observed over less than 5% of the study area at night with minimum coverage at 2000 LST. During phases 3, developing stage of MJO over the western Maritime Continent, maximum rain rates are

observed more frequently at 0500 LST—3 hours earlier than climatological maximum at 0800 LST. On the other hand, the spatial abundance of maximum rates is highest at 0800 LST during phases 5 and 7 as in climatology. Over land, on the other hand, the maximum rain rates are observed at 1700 LST regardless of the phase of MJO (Figure 2.6(b)) and in climatology.

Figure2.7 shows the spatial patterns of the averaged TRMM rain rates over the analysis domain in the morning (0800-1100 LST; (a), (b), (c)) and in the evening (2000-2300 LST; (d), (e), (f)). Among the eight MJO phases, 3 phases of the MJO (phases 3, 5, and 7 in Figure 5) are selected to examine the physical process pertaining to the interaction between MJO and the diurnal cycle of precipitation over the western Maritime Continent. Strong TRMM rain rates over the Java Sea and the ocean adjacent to the northwestern Borneo are evident in Figures 2.7(a) and (b). The maximum rain rate located over the Java Sea between Borneo and the Java Island in phase 3 shifts eastward in phase 5. In phase 7, or the decaying stage of MJO, rain rate prevails over the oceanic region, but their intensity is significantly

reduced (Figure 2.7(c)).

On the contrary, rain rate in the evening is mainly concentrated over islands, such as Borneo, Sumatra, and Sulawesi (Figures 2.7(d), (e), (f)). The strongest rain rate occurs over the northwestern edge of Borneo and Sumatra in phase 3 as shown in Figure2.7(d). In phase 5, the land-ocean contrast of rain rate is reduced noticeably over the Java Sea and rain rate intensity over Borneo and Sumatra also decreases. Similarly, weakened rain rates over land persist in phase 7.

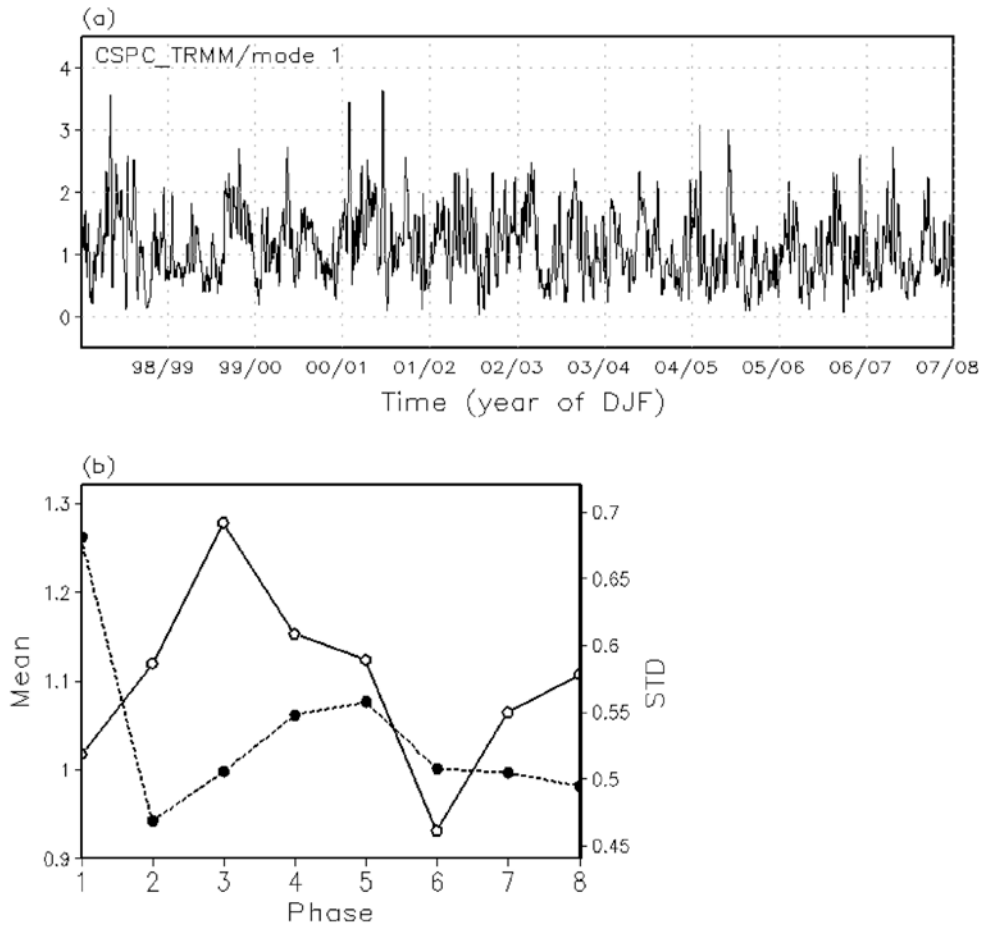

Figure 2.3 (a) PC time series of the first CSEOF of the TRMM rain rate (mm/hr), and (b) the mean (solid) and the standard deviation (dashed) of the PC time series for each phase of the MJO. Cases for which the MJO amplitude is less than 1 were not included in (b).

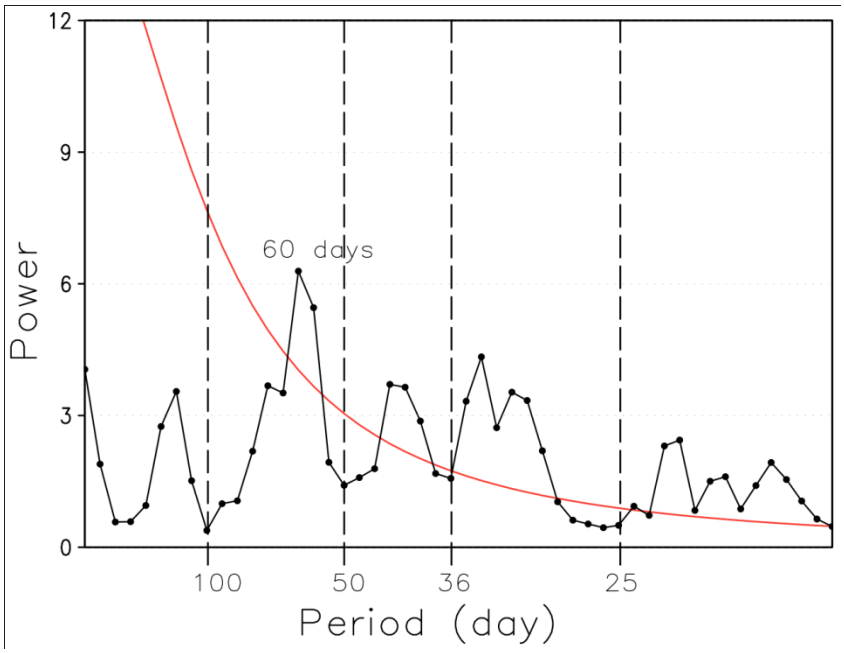

Figure 2.4 Power spectrum for the PC time series of the first CSEOF shown Figure 2.3(a). The red line denotes the spectrum function of red noise with the same variance.

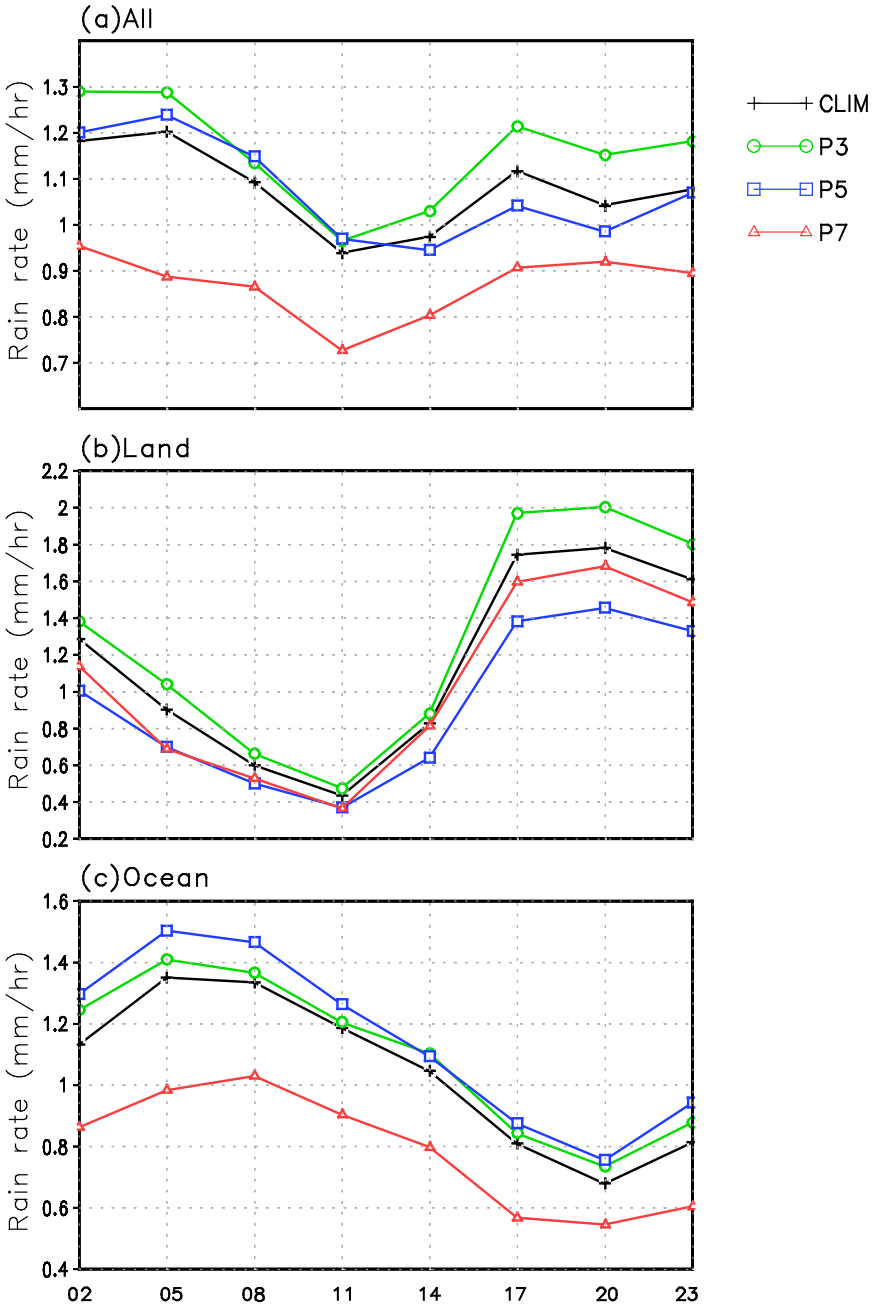

Figure 2.5 Domain averaged diurnal cycle of the TRMM rain rate of climatology and for MJO phases, 3, 5, and 7: (a) for all areas, (b) for land areas, and (c) for ocean areas within the domain. The abscissa denotes the local standard time.

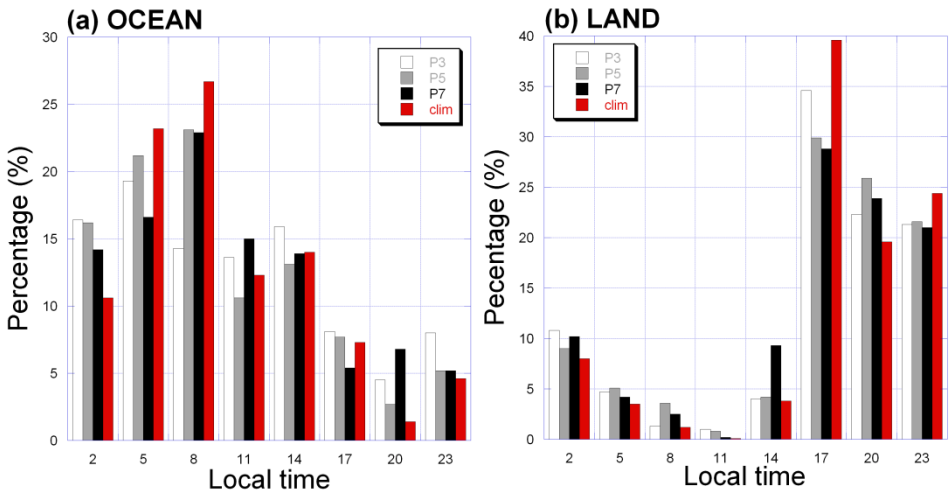

Figure 2.6 Percentage of the area of (a) the ocean and of (b) land recording maximum rain rates at each local time.

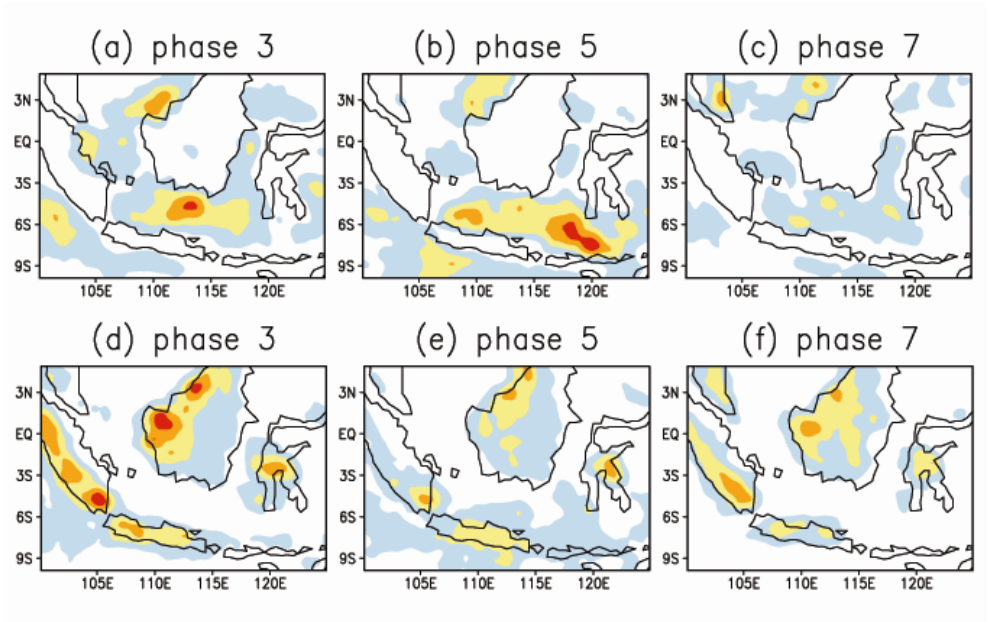

Figure 2.7 Morning (0800-1100 LST) mean TRMM rain rate (mm/hr) for MJO (a) phase 3, (b) phase 5, and (c) phase 7. Evening (2000-2300 LST) mean TRMM rain rate for MJO (d) phase 3, (e) phase 5, and (f) phase 7. The shading interval is 1 mm hr-1 and the zero value isomitted.

2.4 Plausible physical explanations for MJO's modulation of the diurnal cycle

Relevant atmospheric variables are analyzed to delineate how MJO modulates the diurnal cycle of precipitation over land and the ocean respectively. Figure2.8 exhibits the 925 hPa wind speed and the streamline at 0800 LST and 2000 LST of MJO phases 3, 5, and 7 in association with the rain rate in Figure 2.7. The total mean DJF of the 925 hPa wind is subtracted to examine anomalies associated with MJO. The mean state is depicted in Figure 2.9. The overall horizontal circulation pattern of the mean state is consistent with Figure 2 of Johnson and Kriete (1982), which is based on the 1978-79 International Winter Monsoon Experiment (Winter MONEX) over Southeast Asia to define the thermodynamic structure and the circulation feature of the meso-scale cloud systems and their background environment. The Maritime Continent is located downstream of the low-level northeasterly that prevail during the austral summer. In addition, westerly prevails near the equator during the wet season of austral summer (Matsumoto 1992; Hamada et al. 2002; Chang et al. 2004a).

MJO convection is accompanied by westerlies in the western part of the convection and easterlies in the eastern part (Zhang 2005); this feature is displayed clearly in Figure2.8.There are remarkable discrepancies in the magnitude of wind speed according to the different stages of MJO convection. In the developing stage, phase 3, convection accompanying easterlies begins to develop over the western part of the Maritime Continent. Consequently, easterlies counteract prevailing equatorial westerlies resulting in a decrease of wind speed (Figure 2.8(a)). As convection reaches a mature stage, westerlies dominate over most of the analysis domain. Westerlies induced by MJO convection are superimposed on the monsoonal westerlies and give rise to increased wind speeds. This enhancement of the westerlies, in particular, is conspicuous primarily over the oceanic region specifically along the Java Sea (Figure 2.8(b)). As noted in previous studies, topographic blocking over the Maritime Continent tends to cause surface wind to skirt around mountainous islands (Wu and Hsu 2009) and lead to the convergence of flow over the ocean. Westerly flow induced by the MJO persists until phase 7 although its magnitude and spatial extent are

reduced(Figure 2.8(c)).

While horizontal flows associated with the intraseasonal disturbance are clearly depicted in Figure 2.8 with respect to MJO phases, the diurnal variation of wind generated by the land-sea breeze and mountain-valley wind over mountainous Borneo, Sumatra and adjacent oceans causes regional difference between 0800 LST and 2000 LST. While prominently converging flowsare closely related to the nocturnal precipitation over Borneo at 2000 LST in phase 3 and 7, they disappear during phase 5. Strong westerlies seem to disturb the easterlies blowing from the east of Borneo and prevent the convergence over the island.

Figure 2.10 shows divergence anomaly at 925 hPa and pressure velocity anomaly at 500 hPa. Upper panels show clear contrasts of divergence/convergence and downward/upward motion between the land andocean at 0800 LST. Convergence along the Java Sea coincides with the upward motion at 0800 LST particularly in phase 5. Regions of convergence correspond to the areas ofmorning maximum precipitation over the ocean

(Figures2.7(a)-(c)). Strong upward motion and low-level convergence cause heavy rainfall over the Java Sea. On the other hand, intense convergence and strong upward motion are dominant over lands in the evening (2000 LST) as shown in the lower panels. In phase 5, convergence and upward motion over Borneo, Sumatra, and Sulawesi are reduced (Figure 2.10(e)) compared to phases 3 or 7 (Figure 2.10(d) and (f)). This reduction appears to be closely linked to the weakening of the rain rate in Figure 2.7(e) over the land areas. As mentioned above, the enhancement of the westerly flow due to MJO seems to move the location of convergence eastward.

Atmospheric instability defined by the difference of equivalent potential temperatures between 850 hPa and 500 hPa is shown in Figure 2.11 in the context of the MJO phase. Atmospheric condition becomes highly unstable during the mature stage of MJO. Mountainous islands induce flow bifurcation causing near-surface winds to prevail mainly over the oceanic channels between two islands (Wu and Hsu 2009). As a result, heat flux release from the oceans to the atmosphere is enhanced by the increased surface wind leading to instability as described by the wind-induced surface

heat exchange (WISHE) mechanism (Emanuel 1987; Neelin et al. 1987). Due to weakened lower level convergence and vertical motion, strong rain rates are only rarely generated, although strong convective instability is observed over Borneo in the evening during the mature stage (Figure 2.11(e)).

Figure 2.12 shows the diurnal evolution of vertical motion at 500 hPa and lower level divergence at 5°S where Java Sea is located (110°-118°E). Strong upward motion and lower level convergence is confined above the oceanic region in late evening/morning especially during phase 5.

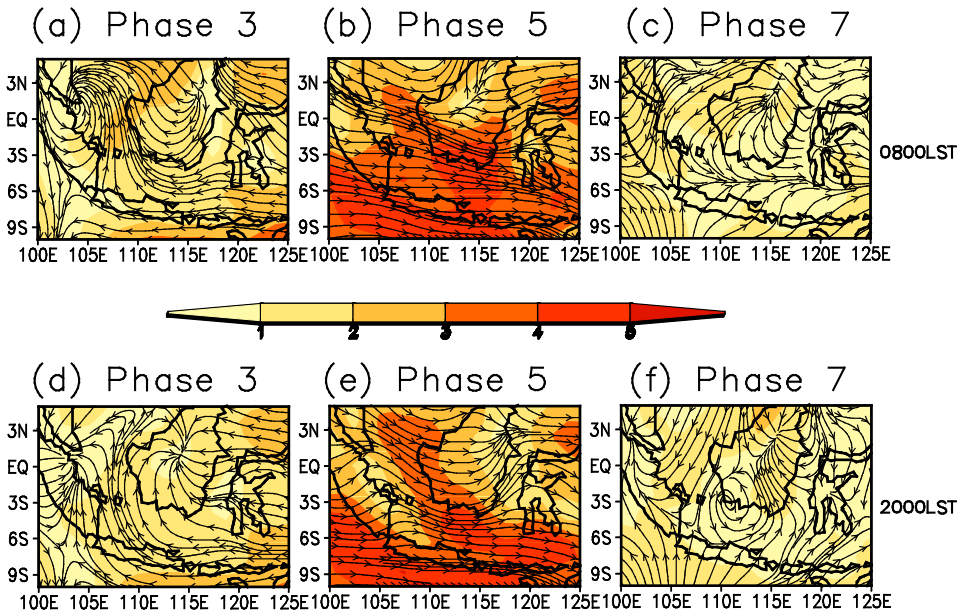

Figure 2.8 Composite maps of anomalous 925 hPa wind speed (shaded, m s-1) and streamline for MJO (a) phase 3, (b) phase 5, and (c) phase 7 at 0800 LST. Panels (d), (e), and (f) are the same as (a), (b), and (c) except at 2000 LST. Ten Austral summers (DJF) mean issubtracted before compositing.

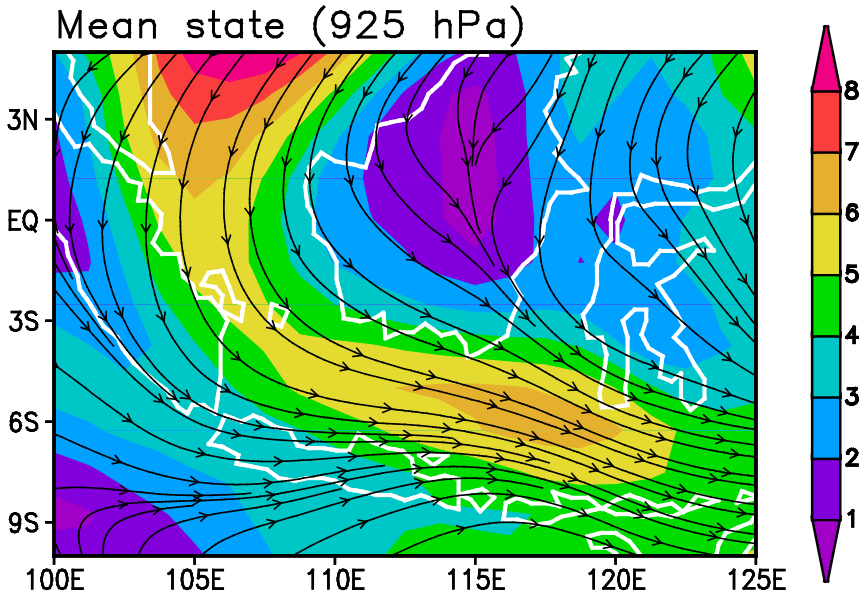

Figure 2.9 The mean patterns of 925 hPa wind speed (shaded, m s-1) and streamlines for 10 Austral summers (DJF).

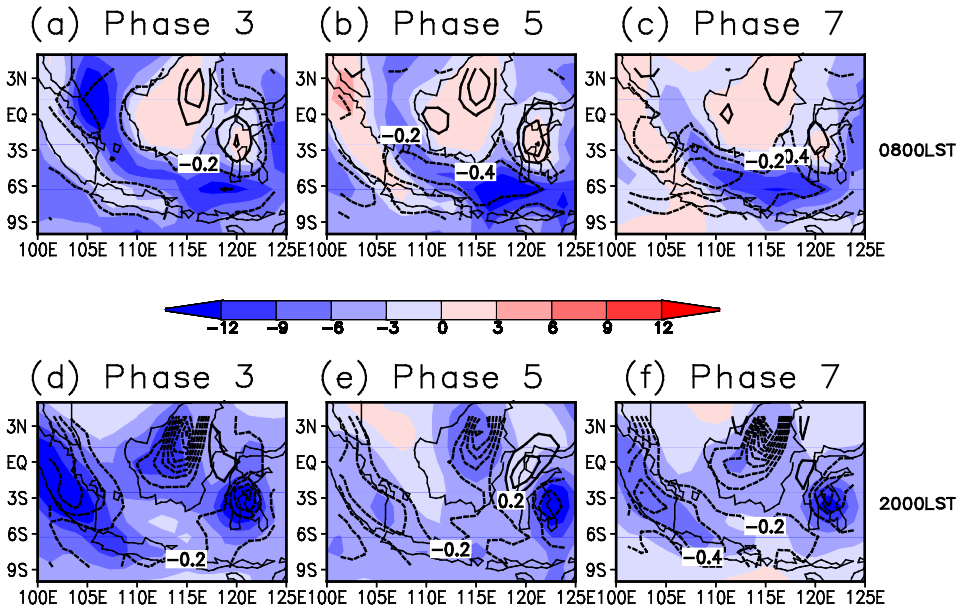

Figure 2.10 Pressure velocity anomaly at 500 hPa (shaded, Pa s-1) and divergence anomaly at 925 hPa (contour, 10-5 s-1) for MJO (a) phase 3, (b) phase 5, and (c) phase 7 at 0800 LST. Panels (d), (e), and (f) are the same as (a), (b), and (c) except at 2000 LST

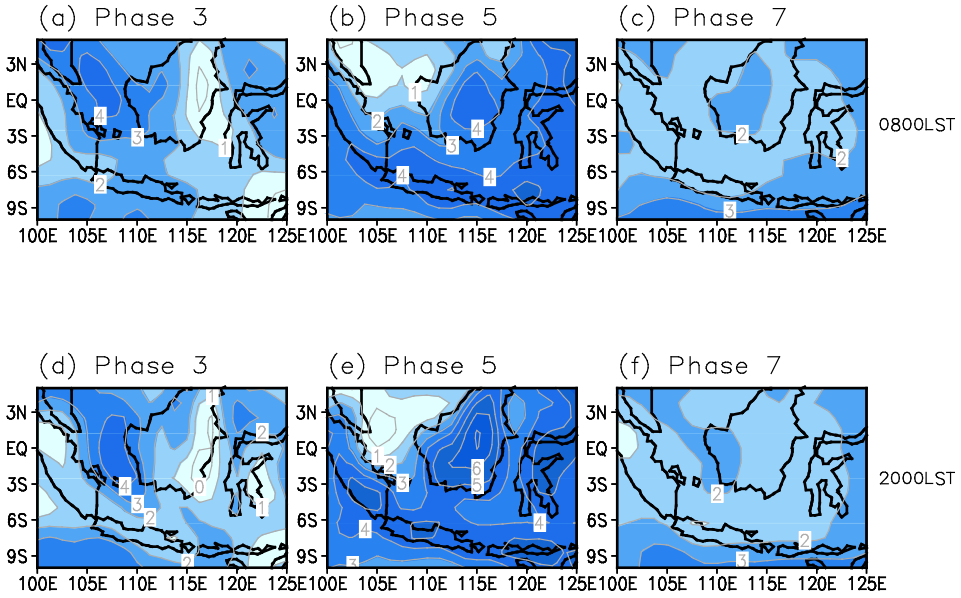

Figure 2.11 Equivalent potential temperature difference between 850 hPa and 500 hPa (K) for MJO (a) phase 3, (b) phase 5, and (c) phase 7 at 0800 LST. Panels (d), (e), and (f) are the same as (a), (b), and (c) except at 2000 LST.

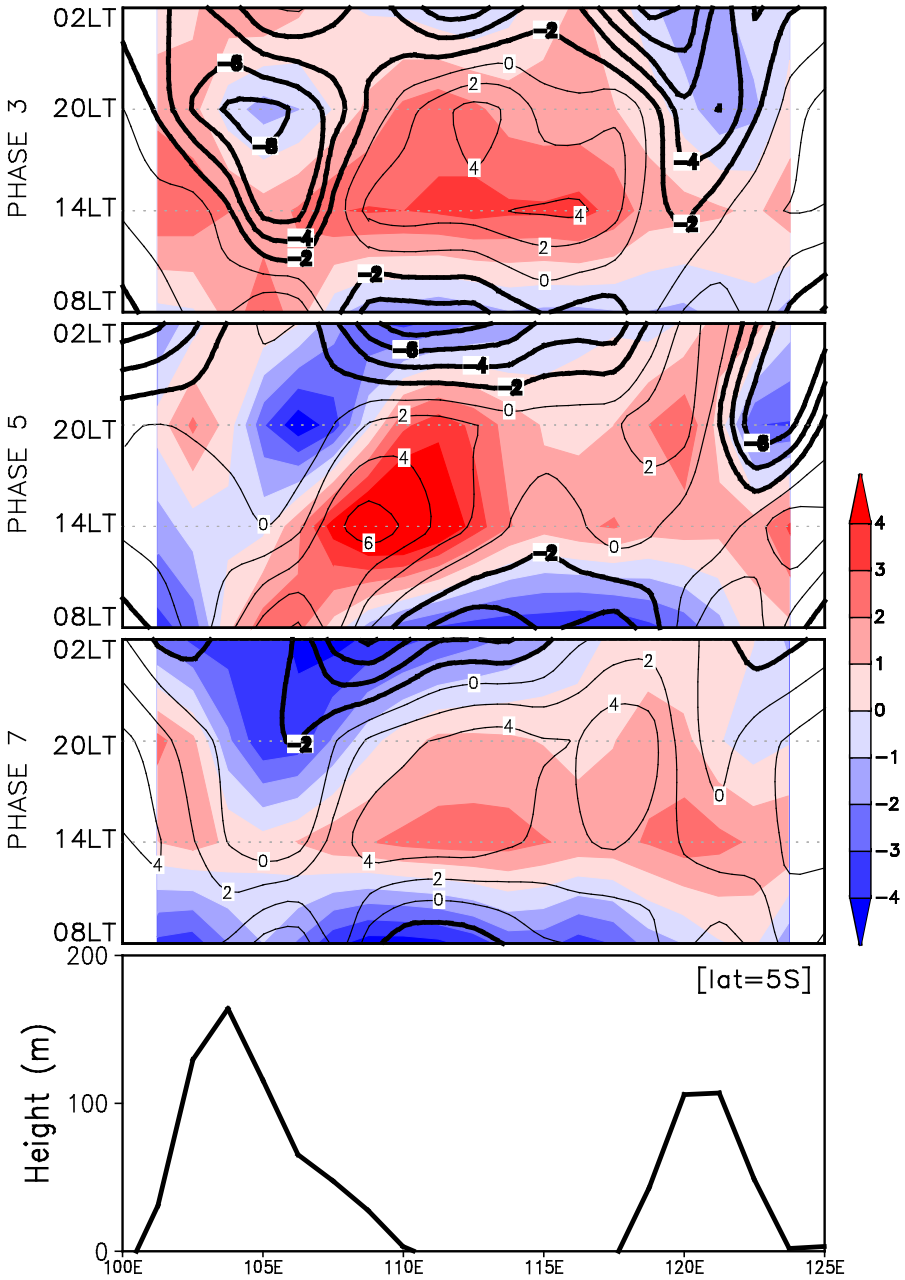

Figure 2.12 Time-longitude plots of pressure velocity at 500 hPa (shaded, Pa s-1) and divergence at 925 hPa (contour, 10-5 s-1) at 5°S for MJO (a) phase 3, (b) phase 5, and (c) phase 7. Vertical velocity was multiplied by 100. Land terrain is described at thebottom panel.

Chapter 3

A Modeling study on the Impact of Diurnal Cycle on the MJO over the Maritime Continent with Assimilation of TRMM Rain Rate into Global Analysis

In this chapter, we evaluate the performance of the Florida State University Global Spectral Model (FSUGSM) with respect to the simulation of the MJO, and investigate the influence of the diurnal cycle on the MJO by adopting applied assimilation techniques. We diminish the diurnal cycle in the model simulation by applying the assimilation technique as described in Section 1.3. Assessment of the performance with respect to the basic climate and intraseasonal oscillation is discussed and climatological characteristics and the impact of the diurnal cycle on the MJO are examined. We show that even small systematic changes in the diurnal cycle can modify the activity of the MJO over the Maritime Continent through the analysis of model experiments. A plausible explanation is also proposed for the influence of the diurnal cycle on the MJO.

3.1.Climatological simulation

First, we investigate the mean state of precipitation as an essential starting point for evaluating model simulations; if the model simulation lacks the correct basic state, then we cannotnecessarily guarantee a better simulation of the MJO (Slingo et al 1996;Kemball-Cook et al 2001). We validate the model simulations against the GPCP observed precipitation during the austral summer (DJF). Both the CTRL and NO_DIURNAL simulations show good agreement with the observed precipitation, although the simulations tend to underestimate the rainfall amounts.

Power spectra analysis is conducted on the time series of rainfall at each grid point (extending from 30° S to 30° N, globally) derived from the CTRL and NO_DIURNAL simulations. Figure 3.2a and Figure 3.2b depict grid points where the diurnal cycle of rainfall has the largest significant power against the red noise background in the CTRL and NO_DIURNAL experiments, respectively. In CTRL, the diurnal component is most dominant over the Maritime Continent, the northern edge of Australia, the middle of South America, and Southern Africa (Fig. 3.2a). In contrast, the

diurnal cycle, which is prominent in CTRL, almost fades out in the NO_DIURNAL experiment (Fig. 3.2b). This implies that because of the assimilation of the daily averaged precipitation and other atmospheric variables into the FSUGSM, the diurnal signal is weakened enough to examine the intraseasonal variability without the diurnal cycle in the NO_DIURNAL simulation. Figure 3.2c displays the CTRL-to-NO_DIURNAL ratio of power in the diurnal band. The power of the diurnal component at greater than the 95% confidence level against the red noise null hypothesis of each grid point from the CTRL and NO_DIURNAL experiments is considered for the ratio. Over 80% of the domain shows the ratio greater than unity. This also supports the suppression of the diurnal cycle in the NO_DIURNAL simulation, especially over the Maritime Continent, which is the main region of interest.

In addition, we summarize the percentage of the region in the analysis domain (40°E–180°E, 15°S–15°N) where the CTRL-to-NO_DIURNAL ratio of not only precipitation but also of relevant variables such as humidity, zonal wind, and temperature exceeds unity in Table 3.1. It turns out diurnal

components are suppressed over most of the analysis region.

Figure 3.3 shows the differences in the DJF mean precipitation between the NO_DIURNAL and CTRL simulations. NO_DIURNAL produces more rainfall than CTRL, especially over the Maritime Continent (marked by the rectangular box in Fig. 3.3) and the middle of South America. Deliberately eliminating the diurnal component in the NO_DIURNAL simulation could closely relate to the increase in the seasonal mean rainfall amount over the Maritime Continent. We deduce that the difference originates from the strong diurnal signal over the Maritime Continent.

We analyze three-hourly precipitation from each experiment, applying CSEOF analysis to ensure that the diurnal signal is suppressedsufficiently in the NO_DIURNAL simulation, and examine how diurnal variations of rainfall over the Maritime Continent are represented in CTRL and NO_DIURNAL, respectively. Figures3.4 and 3.5 display the first CSEOFs, which represent the diurnal cycle of rainfall in the austral summer (DJF) over the Maritime Continent in CTRL and NO_DIURNAL, respectively.

The diurnal rainfall evolution shows a substantial difference between the land and the sea in CTRL (Fig. 3.4). Whereas precipitation over the islands (e.g., Borneo, Sumatra, Sulawesi, and New Guinea) reaches a maximum in the evening (2000–0200LST (Local Standard Time);Fig.3.4 e, f, g) and a minimum in the morning and early afternoon (0800–1400 LST; Fig. 3.4a, b, c), precipitation over the seas (e.g.,the South China Sea andthe Java Sea) reaches its peak in the early morning (0500–1100 LST; Fig.3.4 h, a, b). The rainfall migrations offshore at dawn and inland in the early afternoon are also revealed. These results are consistent with the results of previous studies that were based on different datasets (Kikuchi and Wang 2008; Mori et al. 2004; Ichikawa and Yasunari 2006; 2008;Rauniyar and Walsh 2011). Since the land surface has a lower heat capacity, temperature variation caused by solar heating is moresignificant over the land than over the ocean. However, since we use weekly updated SST as a lower SST boundary condition, this physical process will not be represented completely in model simulations. When the sun rises, the temperature over the land increases rapidly until the sun reaches its maximum altitude. This causes pressure

gradients between the land and the ocean and the static destabilization of the atmosphere (Bowman et al. 2005; Yang and Smith 2006). The situation reverses after sunset.The pressure gradient induces daytime sea breezes, resulting in a moisture supply and a forced ascent of air. The land–sea breeze often plays an important role in the rainfall differences between the land and the ocean in fine temporal and spatial scales (Qian 2008). Remarkably, both the distinct land–sea contrast in the diurnal cycle of rainfall and the propagation of rainfall bandsclearly depicted in CTRL disappear in the NO_DIURNAL simulation (Fig. 3.5). Figure 6 displays one-day averaged precipitation from CTRL. The overall spatial pattern of rainfall in each panel of Fig. 5 is consistent with the rainfall pattern in Fig. 3.6 although the rainfall amounts differ. Therefore, discrepancies between CTRL and NO_DIURNAL are caused by nudging the daily averaged fields in the NO_DIURNAL simulation in an attempt to suppress the diurnal variability.

Table 3.1.Percentage of grid where the CTRL-to-NO_DIURNAL ratio of power in diurnal band greater than unity. (40°E–180°E, 15°S–15°N)

Variables	Percentage (%)
Lower levels integrated MSE	87.4
Vertically iterated MSE	82.4
Precipitation	84.6
Pressure velocity (500 hPa)	92.8
Zonal wind (850 hPa)	97.2
MSE (850 hPa)	78.4
Specific Humidity (1000hPa)	80.7
Temperature (1000 hPa)	98.6
MSE (1000 hPa)	88.2
Evaporation	86.5

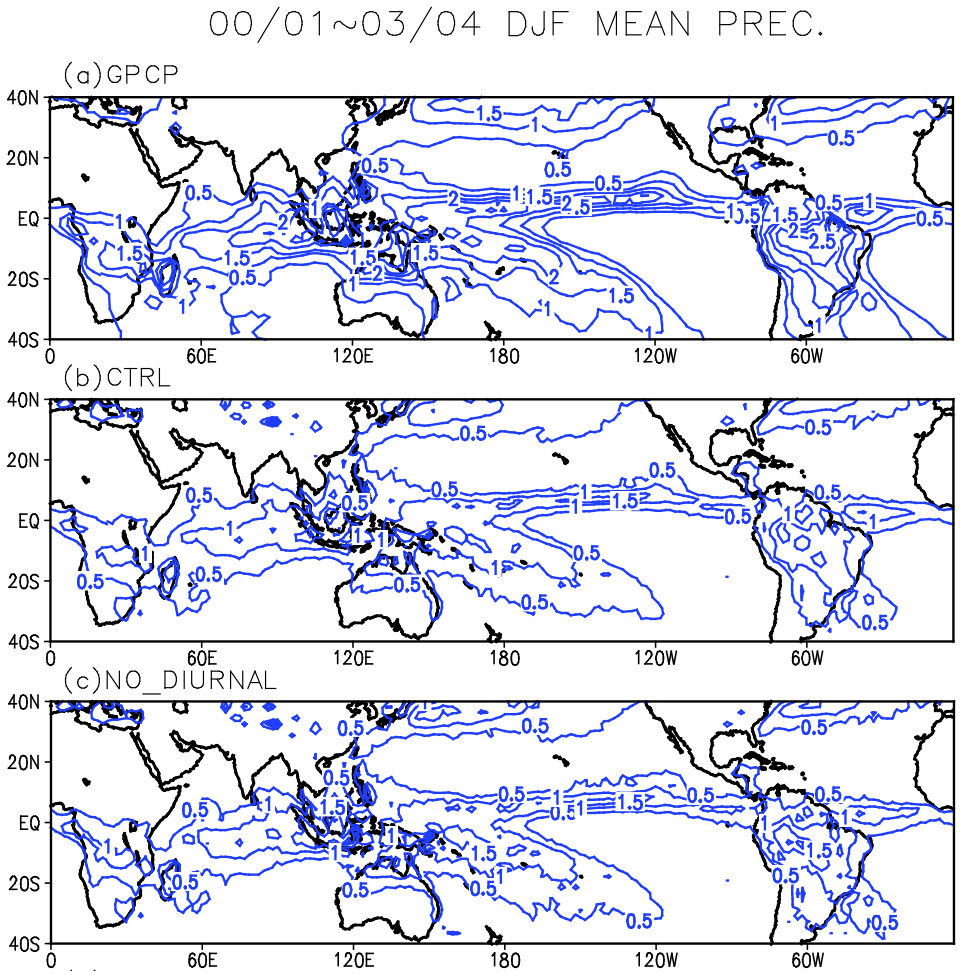

Figure 3.1 Horizontal distributions of austral summer mean (December–February) precipitation (mm day-1) from (a) GPCP, (b) CTRL, (c) NO_DIURNAL. Contours of mean precipitation are plotted every 0.5 mm day-1.

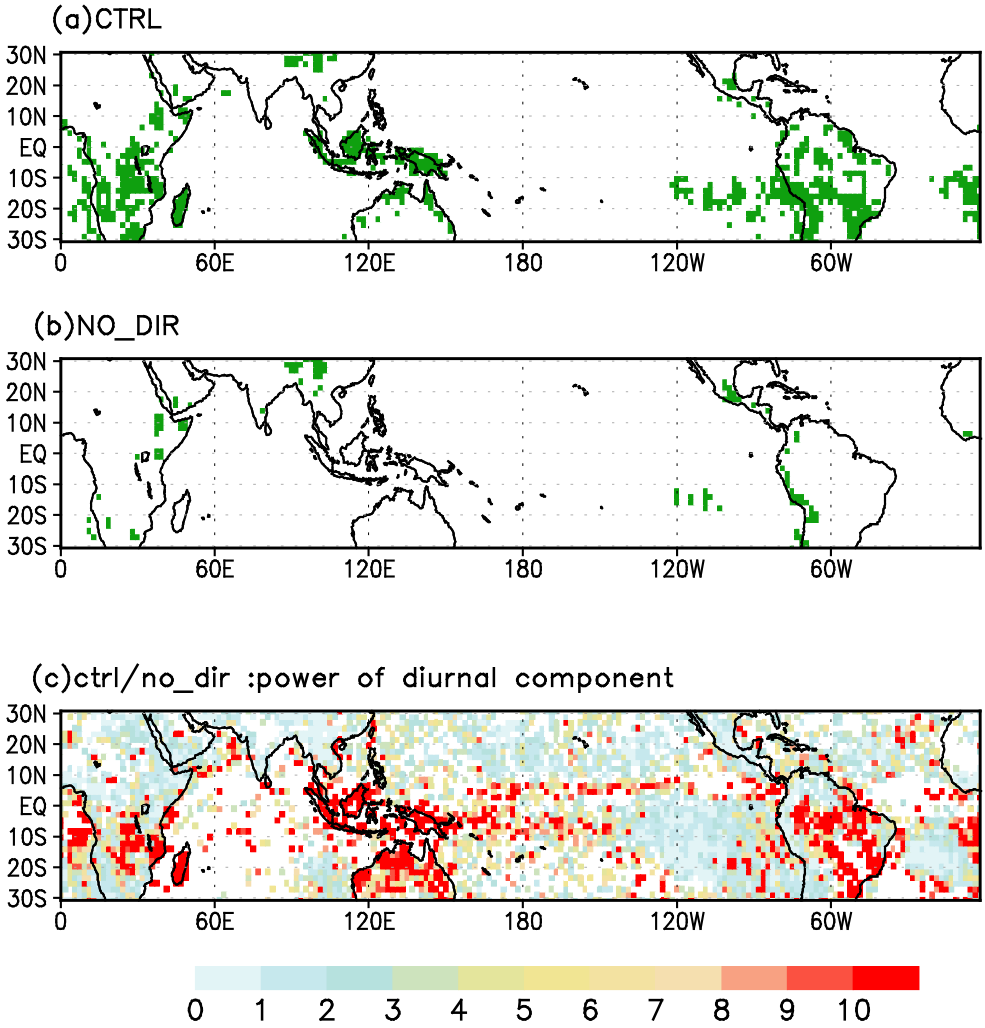

Figure 3.2 Spatial distribution where diurnal component of precipitation has maximum power during boreal winter (DJF) 200/01–2003/04 in (a) CTRL and (b) NO_DIURNAL experiment. The ratio of power at diurnal band of CTRL to that of NO_DIURNAL is shown in (c). The power of diurnal component greater than 95 % confidence level against red noise null hypothesis of each grid point from CTRL and NO_DIURNAL experiment is considered for the ratio.

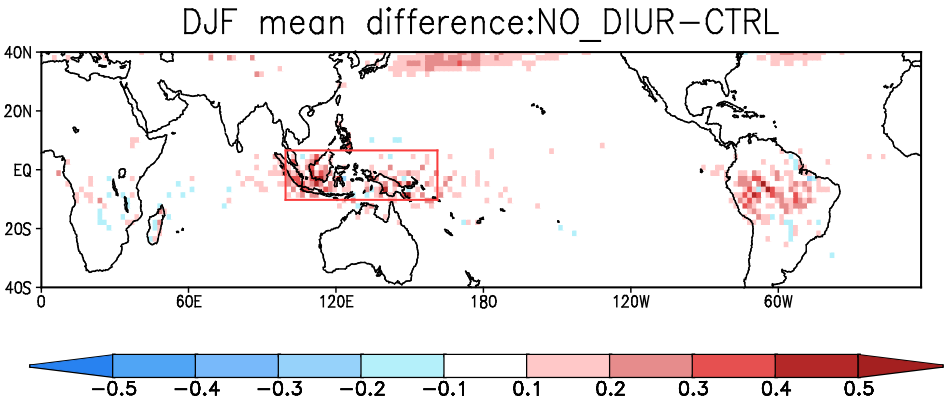

Figure 3.3 Difference in the DJF mean precipitation between NO_DIURNAL and CTRL experiments (mm/day).

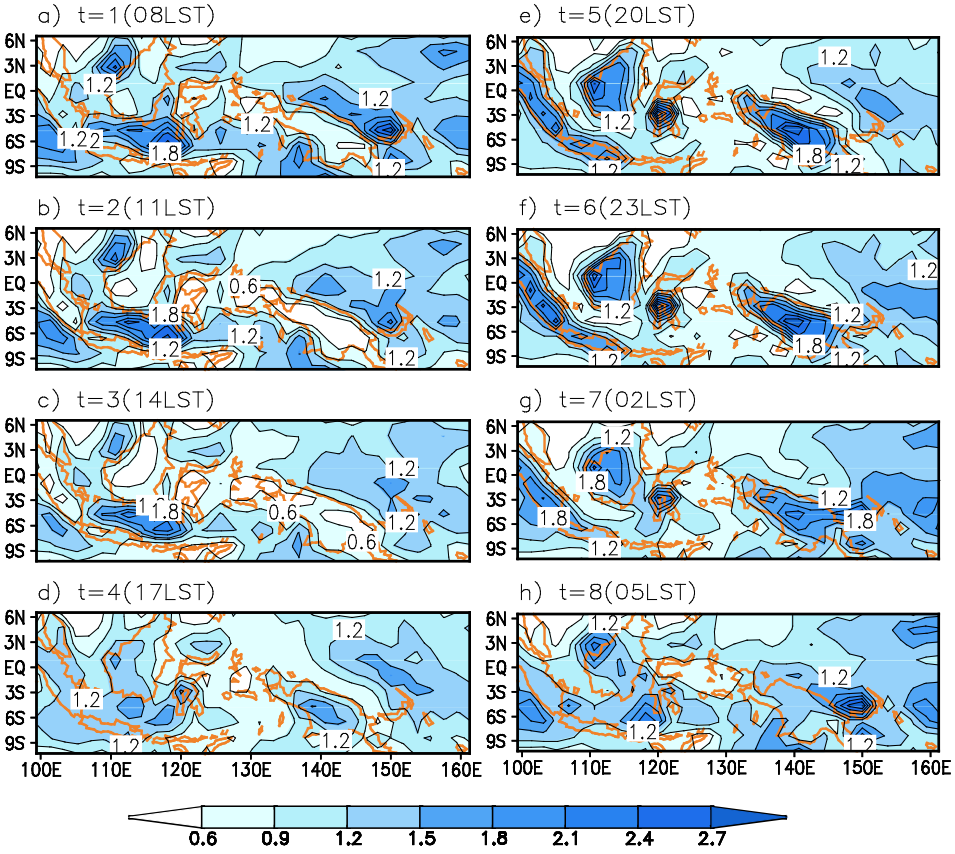

Figure 3.4 Temporal evolution of the CSEOF 1st mode of rainfall distribution (mm/3hr) over the Maritime Continent from CTRL.

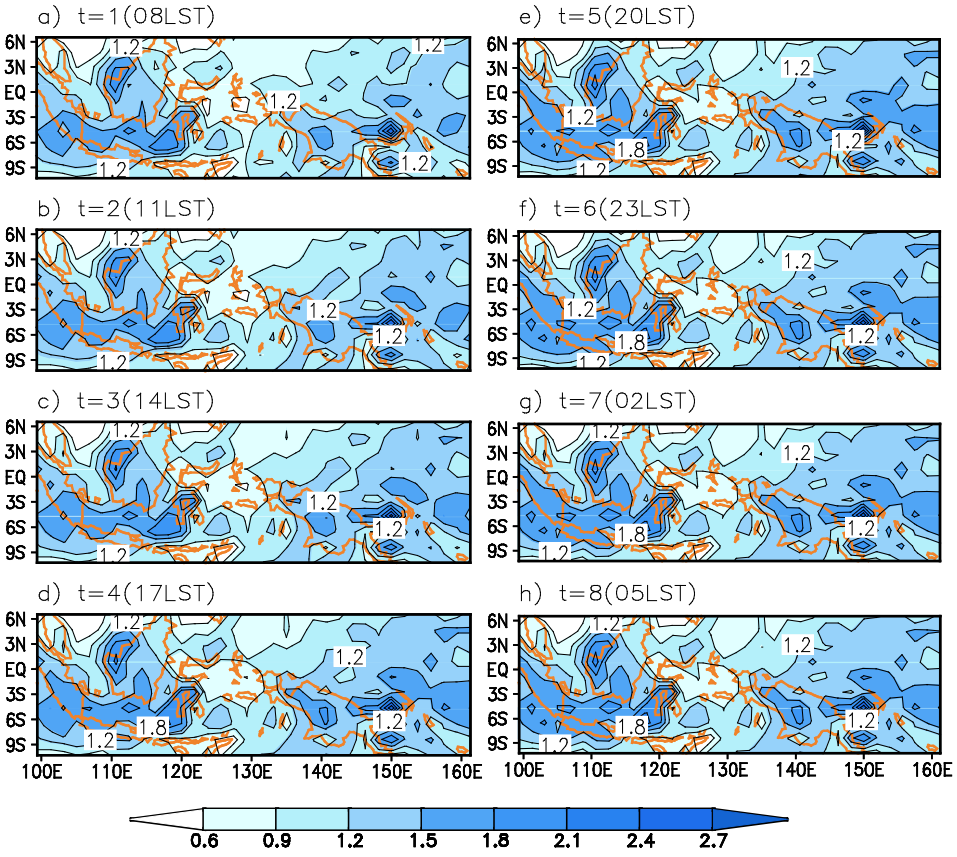

Figure 3.5 Same as Figure 3.4, but from NO_DIURNAL.

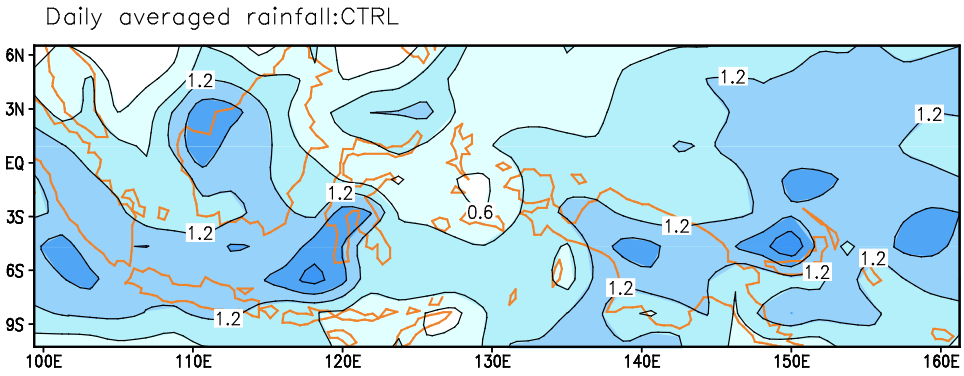

Figure 3.6 The daily averaged CSEOF 1st mode of precipitation (mm/3hr) from CTRL.

3.2. Influence of the diurnal cycle on the MJO

Before focusing on the impact of the diurnal cycle on the MJO, it is necessary to assess the skill of the FSUGSM with the assimilation technique in simulating the intraseasonal oscillation. Figure 3.7 shows the composite spatial patterns of precipitation variability captured by the RMM index. The results from the CTRL experiment (left) are compared to those from the GPCP observation (right). The CTRL composite shows the robust eastward-propagating MJO as being comparable to the MJO in the GPCP data. The salientfeaturesof the MJO are also shown in the CTRL composite (Hendon and Salby 1994; Seo and Kim 2003; Wheeler and Hendon 2004). The MJO convection initiated over the western Indian Ocean in phase 1 propagates eastward and approaches the western part of the Maritime Continent near Sumatra, Borneo, and the Java Sea in phase 3. During phases 3–5, the convectively enhanced phase of the MJO approaches and then resides over the Maritime Continent. In phases 6–8, suppressed convection passes over the Maritime Continent. These DJF composite patterns based on the RMM index show evolutionary features of the MJO similar to features in previous

studies (e.g., Wheeler and Hendon 2004). Therefore, we conclude that the FSUGSM used in this study adequately represents the MJO, allowing us to concentrate solely on the influence of the diurnal cycle regarding the simulation of the MJO.

Figure 3.8 shows phase–longitude diagrams of composite precipitation anomalies of the CTRL (upper) and NO_DIURNAL (lower) experiments. The diagram clearly depicts the origination of the convection anomaliesover the western Indian Ocean and their eastward propagation. Positiveprecipitation anomalies (red) are followed by negative rainfall anomalies (blue). In CTRL, the convective anomaly becomes considerably weaker while passingover the Maritime Continent (100°E–120°E) during phase 3, as a number of previous studies have pointed out (Seo and Kim 2003; Inness and Slingo 2006; Kim et al. 2009), and it redevelops over the west Pacific.In contrast, the weakening of the convective precipitation is absent over the Maritime Continent region in the NO_DIURNAL simulation.

Figure 3.9 shows the difference in composites of precipitation anomalies

between CTRL and NO_DIURNAL with respect to the MJO phase. Of interestare the negative values over the Maritime Continent in phase 3, during which the active MJO convection impinges on the western Maritime Continent (Sumatra, Borneo, and Sulawesi). This implies that compared to the CTRL experiment, more precipitation falls when the convectively enhanced phase of the MJO is located over the Maritime Continent in NO_DIUNRAL. On the other hand, during the suppressed phases of the MJO (phases 5–1), when negative rainfall anomalies reside mainly over the Maritime Continent, the amplitude of these negative anomalies is larger in NO_DIURNAL than in CTRL.

To further examineinfluences that removing the diurnal cycle hason the simulation of the intraseasonal variability in terms of the magnitude and geographical distribution, plots of the variance of 40–80-day filtered precipitation in CTRL and NO_DIURNAL are given in Fig.3.10. This figure can be compared to Fig. 3 of Kim et al. (2009). Their figure is derived for November through April, and they used a 20–100-day bandpass filter to assess the performances of various models in simulating the MJO. CTRL

shows a pattern similar to the CMAP observation in their Fig. 3, resulting in reduced intraseasonal variability over the Maritime Continent (Fig.3.10a). In contrast, large intraseasonal variance extends over the Maritime Continent in the NO_DIURNAL simulation (Fig.3.10b).

Figure 3.11 shows wavenumber–frequency plots (Hayashi 1979) of precipitation and 850-hPa zonal wind in CTRL (Fig.3.11a) and NO_DIURNAL (Fig.3.11b), respectively. The wavenumber–frequency analysis is useful for separating phenomena in the time–longitude domain into westward- and eastward-moving components (Wheeler and Kiladis 1999). Using this method,we interpret dynamical attributes of deep tropical convection regarding the dispersion relations of particular wave modes. Zonal wavenumbers 1–3 are evident in precipitation and zonal wavenumber 1 is dominant in zonal wind at 850 hPa for periods of 45–50 days in CTRL and NO_DIURNAL. This result is quite similar to the observational result of Kim et al.(2009). Waves within these scales can be considered the MJO (Wheeler and Kiladis 1999). Worth noting is that the assimilation of the daily averaged fields has no impact on periods of dominant waves; however,

it does affectthe power of rainfall. Comparing the power of rainfall and the zonal wind at 850 hPa for periods of 45 to 50 days between CTRL and NO_DIURNAL, we findan increase in the power of rainfall in NO_DIURNAL compared with CTRL. We find no significant change in the power of zonal wind at 850 hPa in either experiment. Fromthese results, we deduce the removal of the diurnal component exerts more direct influence on the thermodynamic process rather than on the dynamic process related to the evolution of the MJO.

We analyze divergence, specific humidity, zonal wind, and pressure velocity anomalies relevant to the MJO. Composite variables averaged over the Maritime Continent with respect to phase are shown in Fig.3.12. Time series exhibit general aspects of dependency onthe evolution of the MJO convection. For example, when convection starts to develop in phase 3 over the Maritime Continent, the wind begins to change from easterly to westerly, as observed in previous studies (e.g., Seo and Kim 2003), and lower level convergence and upward motion at 500 hPa intensify, accompanied by an increase in the humidity. In comparison with CTRL, as

pointed outabove, area-averaged precipitation from the NO_DIURNAL experiment increases during the active phases (3–4) of the MJO. Analogously, vertical motion at 500 hPa, convergence at 1000 hPa, and specific humidity at 700 hPa in the NO_DIURNAL experiment have larger values than those same variables from CTRL during convectively active phases (Fig.3.12c, d, e). In contrast, zonal wind at 850 hPa shows little difference between the NO_DIURNAL and the CTRL experiments regardless of phase.

These results suggest that the deliberate suppression of the diurnal signal during the integration gives rise to an amplification of the MJO without changing propagating speed, especially over the Maritime Continent where the prominent diurnal cycleexists. Because the same wind and convection are nudged toward observation and reanalysis in the daily time scale, the propagation speed cannot be changed by the experimental design.

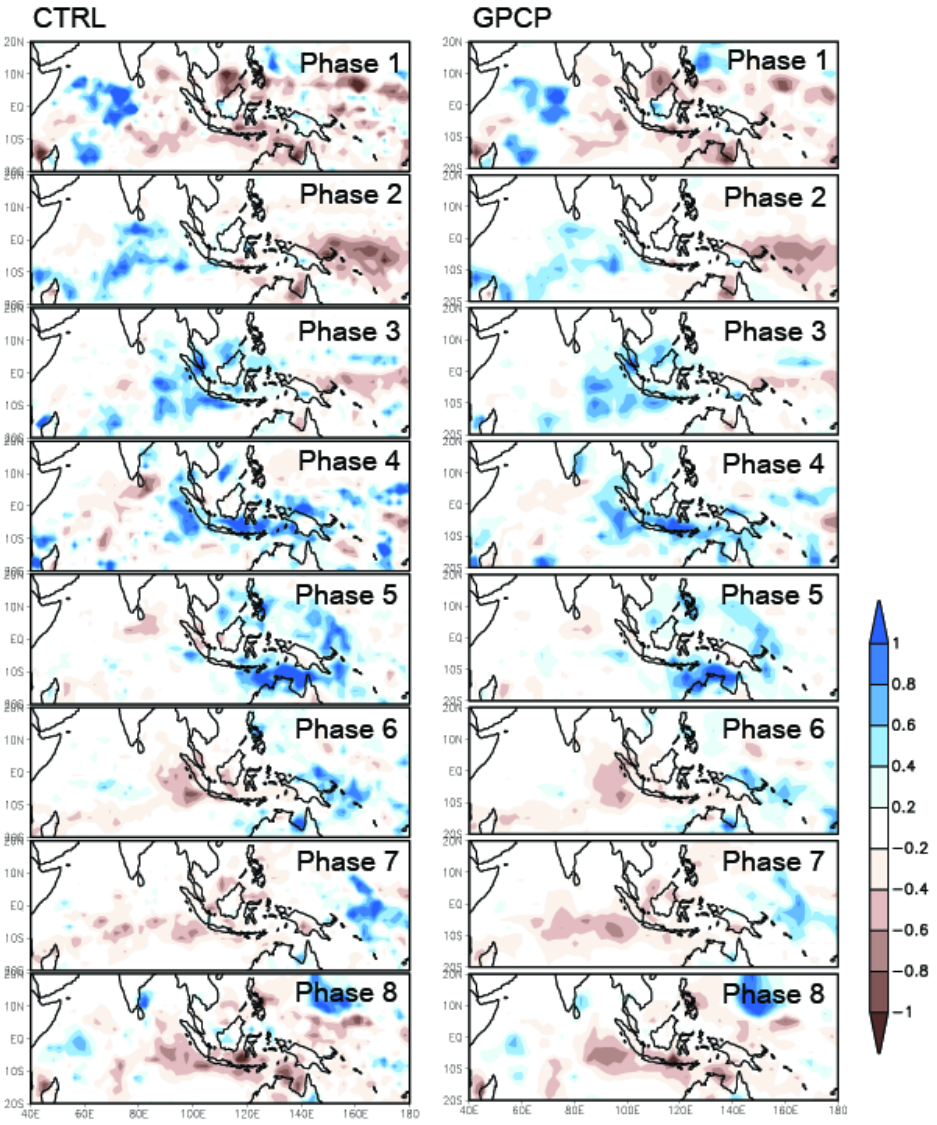

Figure 3.7 DJF composite precipitation anomalies (mm/day) of CTRL experiment (left) and GPCP observation (right).

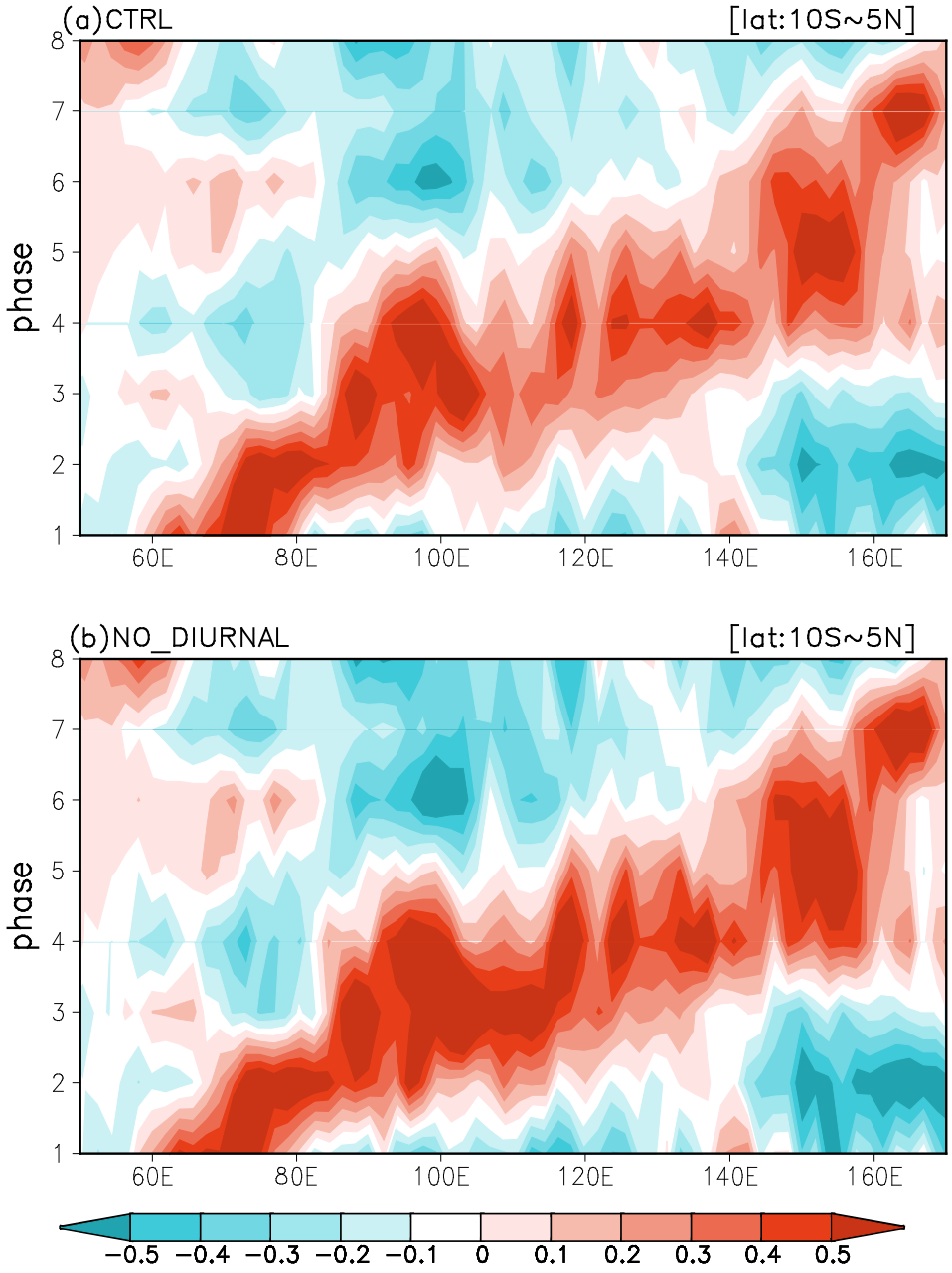

Figure 3.8 Phase–longitude diagrams of composite precipitation anomalies (mm/day) of (a) CTRL and (b) NO_DIURNAL experiments. Phases are from the MJO life cycle composite and values are averaged between 10°S and 5°N.

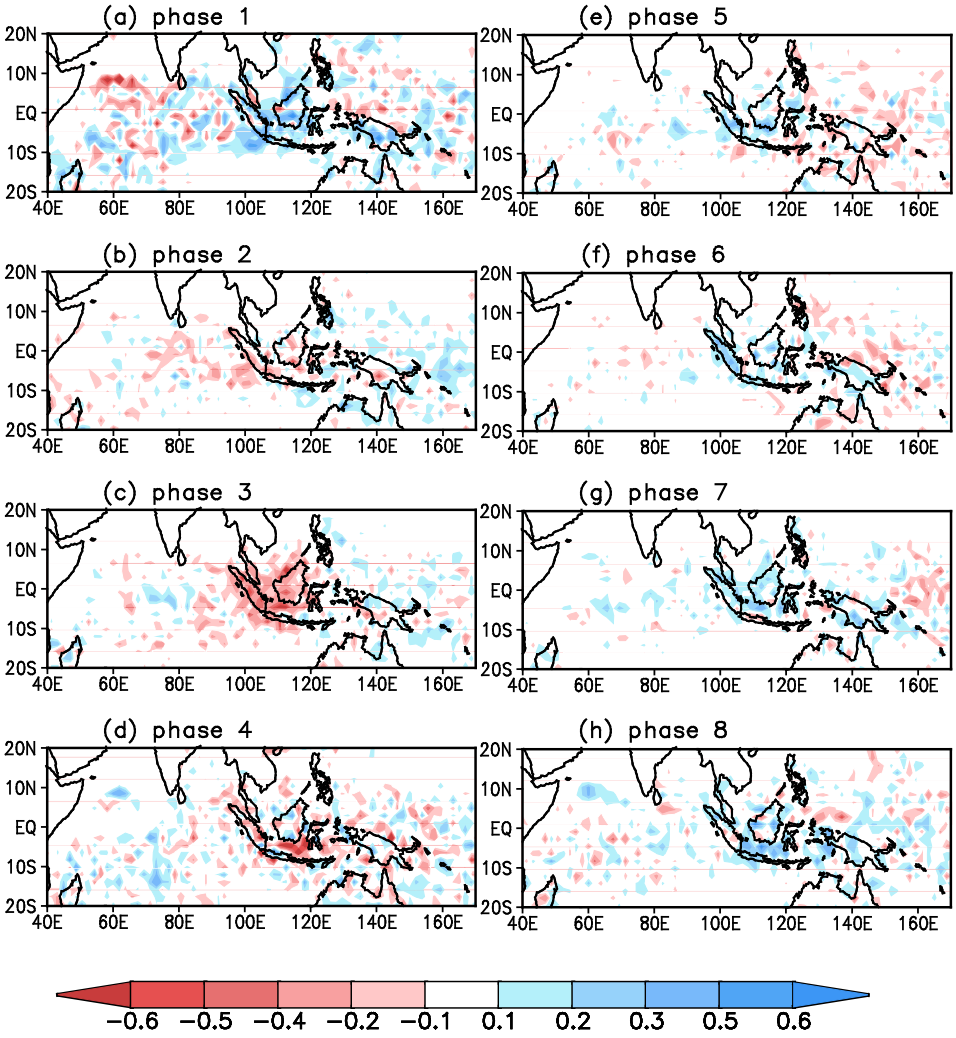

Figure 3.9 Spatial distribution of the difference in composite precipitation anomalies (mm/day) between CTRL and NO_DIURNAL with respect to the MJO phase.

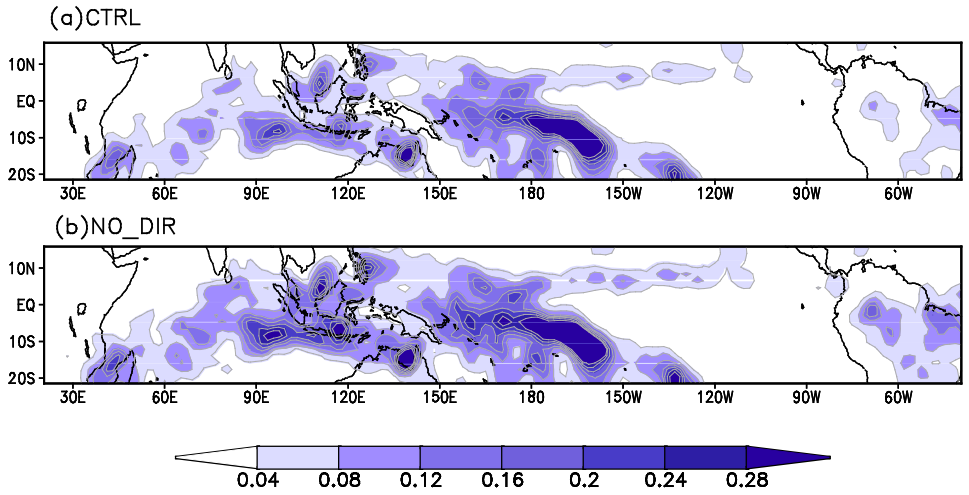

Figure 3.10 Variance of 40–80 day bandpass filtered precipitation (mm2/day2) during austral summer (DJF) 2000/01–2003/04.

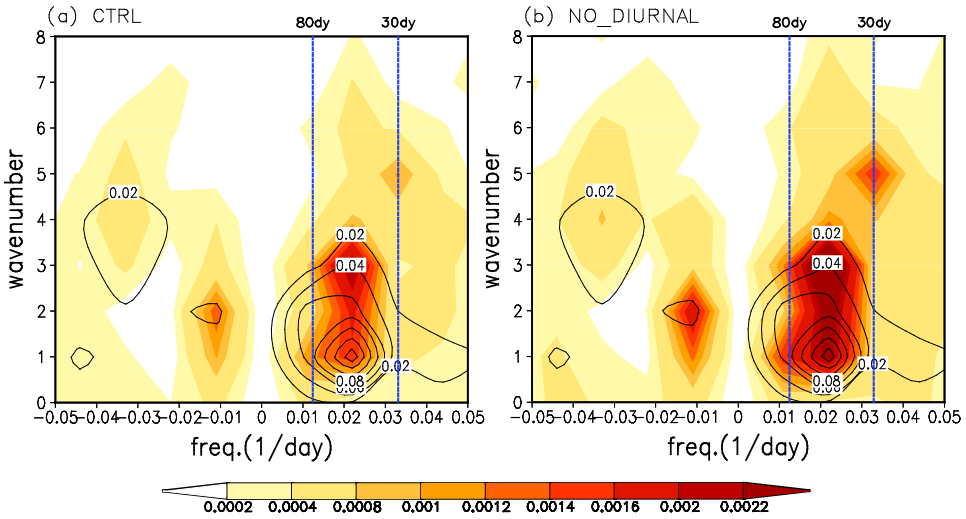

Figure 3.11 DJF wavenumber–frequency spectra of 10°S–10°N averaged precipitation (mm2/day2) (shaded) and 850-hPa zonal wind (m2/sec2) (contour) for (a) CTRL and (b) NO_DIURNAL simulation.

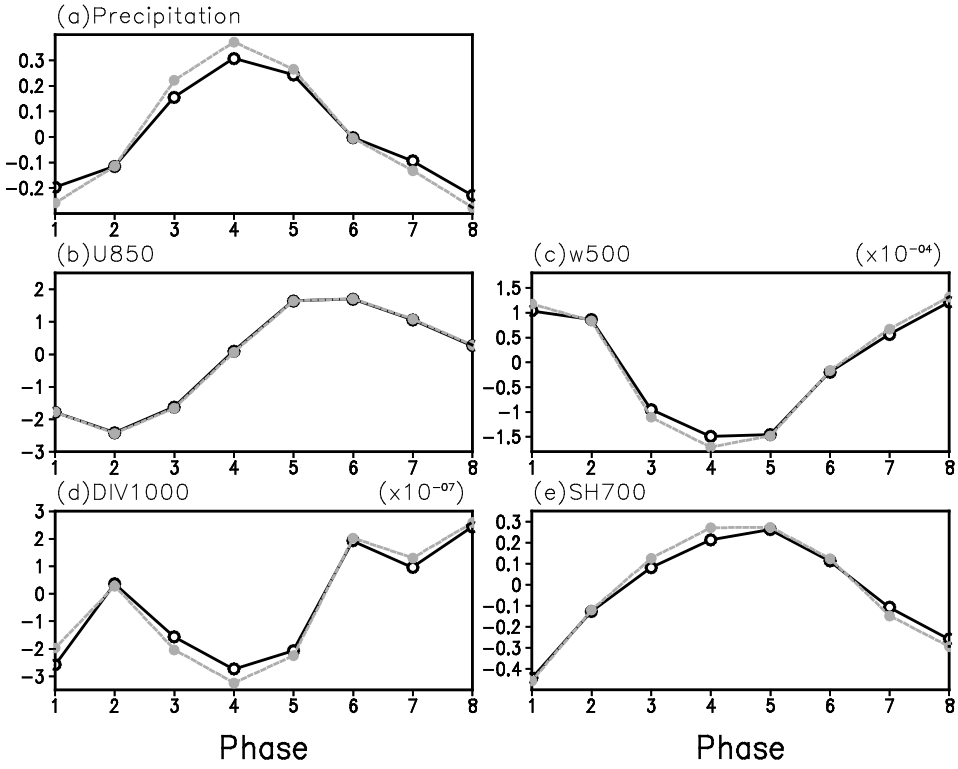

Figure 3.12 Composite variables averaged over the Maritime Continent (10°S–5°N, 100°E–160°E) from CTRL (black solid line) and NO_DIURNAL (grey dotted line) with respect to the MJO phase: (a) precipitation (mm/3hr), (b) zonal wind (m/sec) at 850 hPa, (c) pressure velocity (Pa/sec) at 500 hPa, (d) divergence at 1000 hPa (/sec), and (e) specific humidity (kg/kg) at 700 hPa. Seasonal cycles are all removed before composites.

3.3. How does the suppressed diurnal cycle affect the mean state of rainfall?

Since it is well known that simulation of the MJO is linked with that of the background mean state (Slingo et al. 1996), we started our research by comparing the simulations of mean state by CTRL and NO_DIURNAL, shown in Figs. 3.1 and 3.3. As a result, we find that the simulation with a suppressed diurnal cycle reproduces a larger amount of the mean precipitation over the Maritime Continent than does the simulation with the general diurnal cycle. Prior to performing the detailed analysis on the impact of the modulation of the diurnal cycle on the MJO simulation, it is essential to investigate the physical mechanism behind the increase of seasonal mean precipitation in the NO_DIURNAL experiment. Since cumulus parameterization in the model plays the most important role in the precipitation process, it is helpful to examine the convective instability and moisture convergence, which are key components of the modified Kuo scheme used in this study.

First, we compare convective instability, defined as the difference between

equivalent potential temperature at 500 hPa and 850 hPa (Sato and Kimura 2005), as shown in Fig. 3.13. Larger vertical differences of equivalent potential temperature over the Maritime Continent are more prevalent in NO_DIURNAL than in the CTRL simulation, which indicates more conditional instability exists in the NO_DIURNAL simulation. Figure 3.14 shows diurnal variation of the convective instability in the CTRL experiment (left column: a, b, c, d) and in the NO_DIURNAL experiment (right column: e, f, g, h). In the CTRL experiment, the air above the land areas of the Maritime Continent becomes unstable at 06 UCT, which corresponds to approximately 14 LST. The convective instability provides favorable conditions for late afternoon precipitation over land areas as shown in Fig. 3.4d, e, f, g. On the other hand, the assimilation of the daily averaged variables from reanalysis and rain rates results in persistence of convective instability all day long, even though instability increases at 06UTC over the land areas of the Maritime Continent.

Second, Fig. 3.15 shows the diurnally varying moisture convergence along with the differences of the magnitude between the CTRL and the

NO_DIURNAL experiments. From 00 UTC to 06 UTC, NO_DIURNAL simulates stronger moisture convergence over the Maritime Continent than the CTRL run does. However, from 12 UTC, which is when late afternoon and evening rainfall occurs over the land, the moisture convergence over Sumatra, Java, and New Guinea in CTRL becomes stronger than the convergence in the NO_DIURNAL simulation. Figure 3.16 presents the overall increase of moisture convergence in NO_DIURNAL compared to the CTRL run during the analysis period. On the basis of these results, we speculate that convective instability and moisture convergence are quite evenly distributed in time because the assimilation of daily averaged values during model integration of NO_DIURNAL differs from the CTRL simulation, which resolves distinct diurnal change of convective instability and moisture convergence. As a result, the assimilation of the daily averaged variables seems to satisfy the requirements, e.g., convective instability and moisture convergence (Nune and Cocke 2004) for physical initialization, which enables more frequent assimilation of moisture. Accordingly, this more frequent assimilation of moisture may contribute to the increase of

mean precipitation over the Maritime Continent in the NO_DIURNAL simulation.

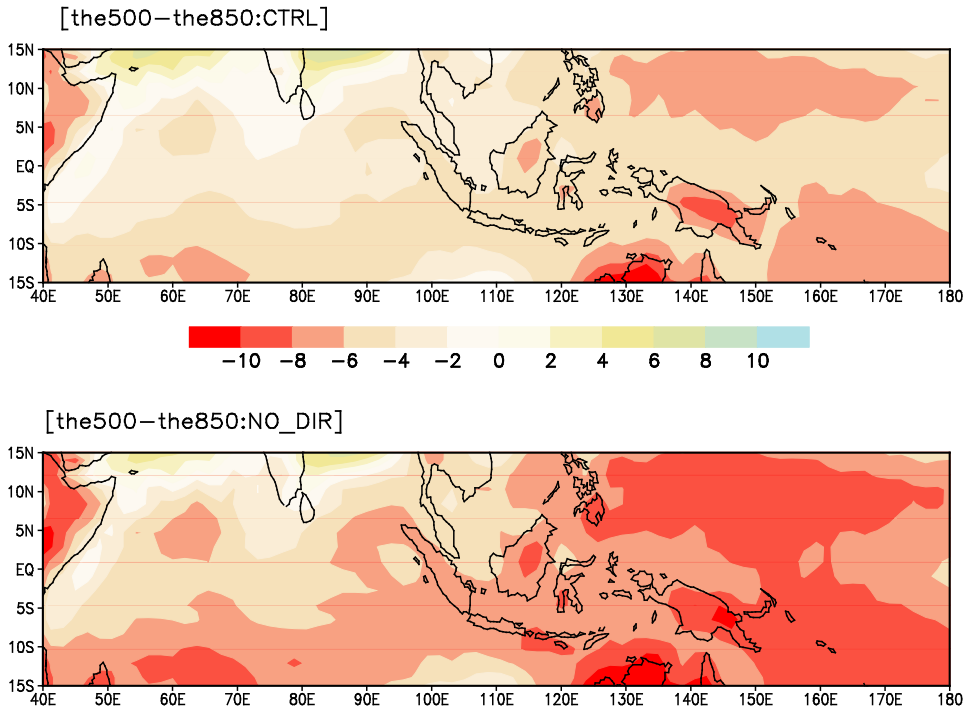

Figure 3.13 Convective instability, defined as the difference of the equivalent potential temperature at 500 hPa and 850 hPa, in CTRL (top) and NO_DIURNAL (bottom) averaged during boreal winter (DJF) 200/01–2003/04.

.

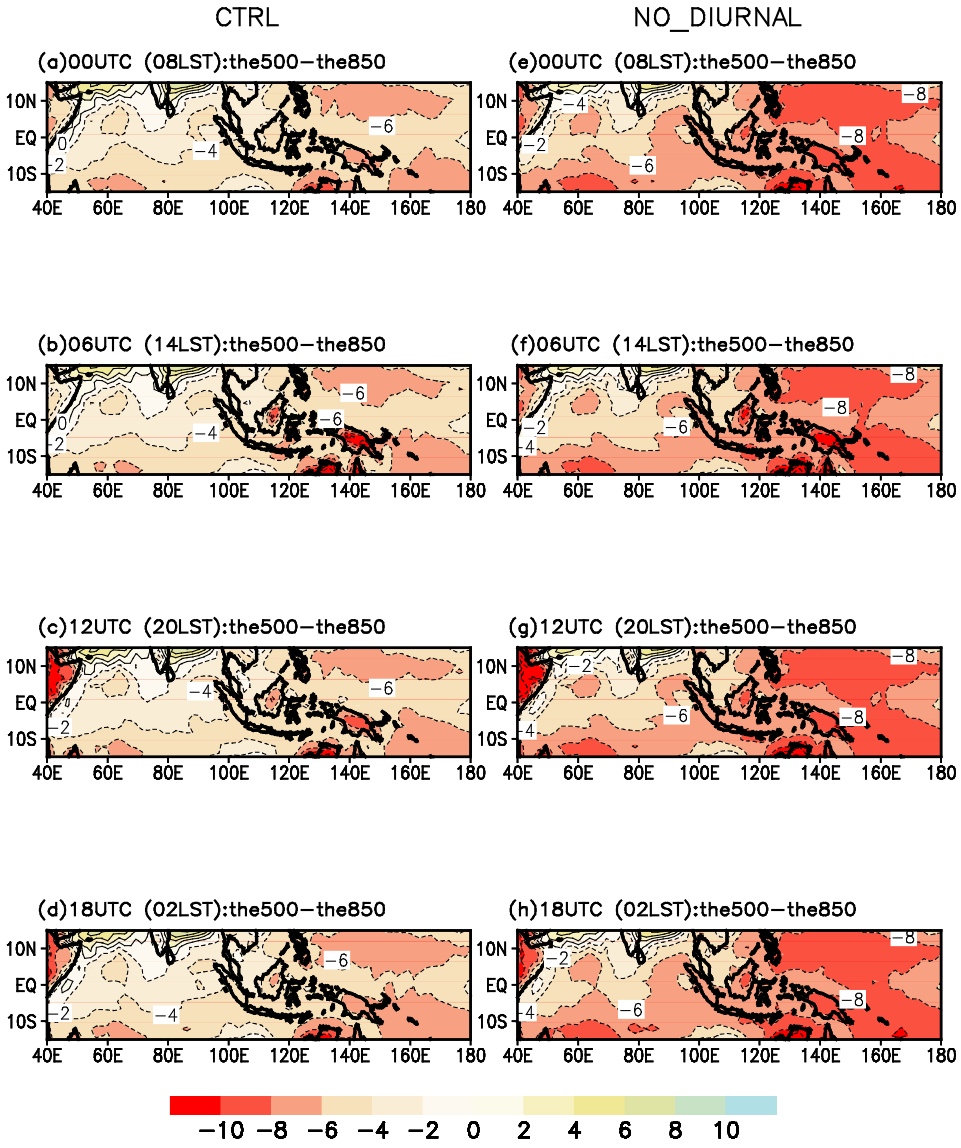

Figure 3.14 Diurnal variation of convective instability (K) in CTRL (a) –(d) and NO_DIURNAL (e) –(h) during boreal winter (DJF) 200/01–2003/04. The time in parenthesis denotes the corresponding local time of MaritimeContinent.

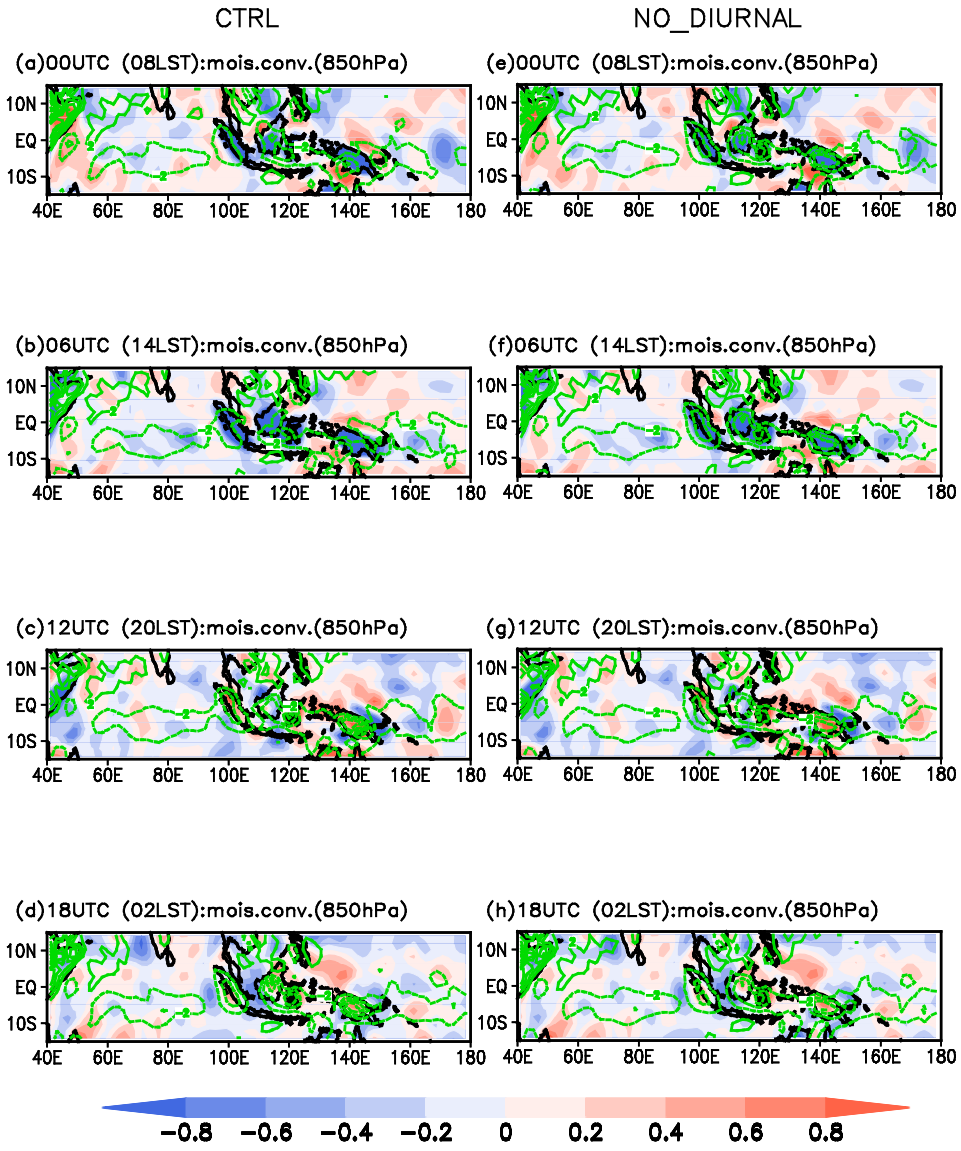

Figure 3.15 Diurnal variation of moisture convergence at 850 hPa (contour: 10-5 g/kg/sec) in CTRL (a)~(d) and NO_DIURNAL (e)~(h) during boreal winter (DJF) 200/01–2003/04. The time in parenthesis denotes the corresponding local time of Maritime Continent. Zero lineis omitted. The shaded areas denote corresponding difference of magnitude of moisture convergence between CTRL and NO_DIURNAL experiment at each time.

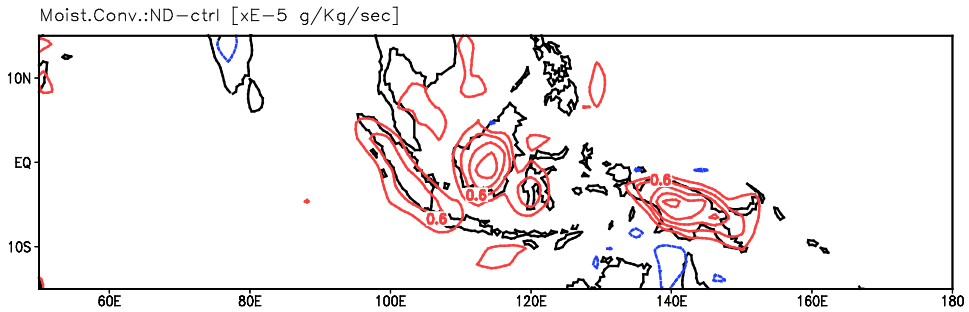

Figure 3.16 Difference of magnitude of moisture convergence between NO_DIURNAL and CTRL experiment averaged during boreal winter (DJF) 200/01–2003/04.

3.4. How does the suppressed diurnal cycle maintain the amplitude of the MJO over the Maritime Continent?

Using the detailed comparison of the MJO produced by the CTRL and NO_DIURNAL model simulations, we have demonstrated that diminishing the diurnal cycle during the model integration does produce an intensified MJO over the Maritime Continent. The question then becomes, which driving mechanism causes this difference? To answer the question, we must consider the theories regarding the development of MJO convection. Although theories based on observations and modeling studies have been suggested to explain the development of the MJO and its characteristics, fundamental understanding of the physical mechanism underlying the MJO remains elusive (Zhang 2005). A recharge-discharge theory (Bladé and Hartmann 1993) is one of the possible mechanisms that explains the evolution of the MJO. According to the paradigm, buildup of a column of moist static energy (MSE) occurs before MJO deep convection, and MSE is discharged during and after MJO convection (Bladé and Hartmann 1993;Kemball-Cook and Weare 2001; Maloney 2009). MSE is defined as

$h = C_pT + gz + Lq$ where C_p is the specific heat of air, T is air temperature, g is the gravitational constant, z is the geopotential height, L is the latent heat of condensation, and q is the specific humidity. The first term on the right side of MSE denotes the enthalpy per unit mass of air. The second term is the potential energy, and the third term is the latent heat content. The first two terms stand for the dry static energy. When air rises dry adiabatically, enthalpy is converted into potential energy and latent heat content remains constant. In saturated adiabatic ascent, energy is exchanged among all three terms. While the enthalpy and latent heat decrease, potential energy increases. Therefore, MSE is a useful property for examining the energy available to a parcel in the convective area on the basis of moisture and temperature in terms of not only the MJO but also the diurnal cycle. MSE is approximately conserved in theair parcels, even as they undergo phase changes between vapor and liquid, including the precipitation process (Beck and Bretherton 2006). Atmospheric convection vertically rearranges MSE, but does not affect the column-integrated MSE.

Figure 3.17 shows the composite vertical distribution of the intraseasonal

MSE anomalies at 115°E as a function of the MJO phase. Recall the result presented in Fig. 8 showing an apparent discrepancy between CTRL and NO_DIURNAL in the amount of rainfall anomalies near 115°E at phase 3. The overall vertical distributions are quite similar to those explained by previous studies (e.g., Kemball-Cook and Weare 2001; Maloney 2009) and in agreement with the recharge–discharge theory of the MJO. Positive MSE anomalies appear at lower levels (1000 hPa–950 hPa) in advance of the rainfall peak (phases 1–2). At phase 3, these anomalies build upward to 850 hPa. Positive anomalies in MSE peak in the middle troposphere at phase 4 consistent with the phase of the maximum positive precipitation anomalies over the Maritime Continent. Negative MSE anomalies reach their maxima at phase 6, during which the peak in negative rainfall anomalies occurs over the Maritime Continent, as shown in Fig. 3.8. A noticeable difference of magnitude in positive MSE anomaly peaks exists between CTRL and NO_DIURNAL in the lower troposphere. The MSE anomaly peak in NO_DIURNAL is 450 J kg^{-1} at 850 hPa during phase 3, which is 100 J kg^{-1} larger than the anomaly peak in CTRL. According to Kemball-Cook and

Weare (2001), the MJO is partially controlled by the buildup and discharge of the low-level MSE. Therefore, Fig. 3.14 suggests that the larger positive MSE anomalies in NO_DIURNAL contribute to the intensification of the MJO over the Maritime Continent.

We also investigate the convective instability over the Maritime Continent in terms of the evolution of the MJO in Fig. 18. The upper panel in Fig. 3.18 shows the composite of the absolute values after subtracting the convective instability of CTRL from that of NO_DIURNAL at MJO phase 3. A wider range of the larger conditional instability exists in NO_DIURNAL compared to the CTRL simulation. The lower panel in Fig. 3.18 shows the variation of the convective instability over the Maritime Continent in each simulation with respect to the MJO phase. The larger the absolute value exhibited by the time series, the more unstable the condition it indicates. Whereas stronger instability occurs during the developing and enhanced MJO phases (1–3), the instability decreases when suppressed MJO convection approaches the Maritime Continent at phase 6. The NO_DIURNAL maintains stronger convective instability than CTRL does

throughout the MJO life cycle. The difference of the instability has maximum value during phase 3 consistent with the increase of the MSE difference shown in Fig.3.8.

Moisture convergence in the boundary layer is one of the important factors that provides favorable conditions for the development of MJO convection (Maloney and Hartmann 1997; Zhang 2005). Low-level convergence provides an upward flux of moisture by increasing the low-level equivalent potential temperature through moistening (Seager and Zebiak 1994). We compute the difference of the moisture convergence at 850 hPa between the NO_DIURNAL and the CTRL experiments (Fig. 3.19). Moisture converges more strongly over the Maritime Continent in NO_DIURNAL than it does in the CTRL simulation. Larger instability and stronger moisture convergence provide a condition conductive for the development of convection.

Thus, the amplification of the MJO over the Maritime Continent in the NO_DIURNAL experiment may be inferred from the combined effect of

the increased buildup of MSE, a more convectively unstable condition, and stronger moisture convergence revealed in the NO_DIURNAL simulation.

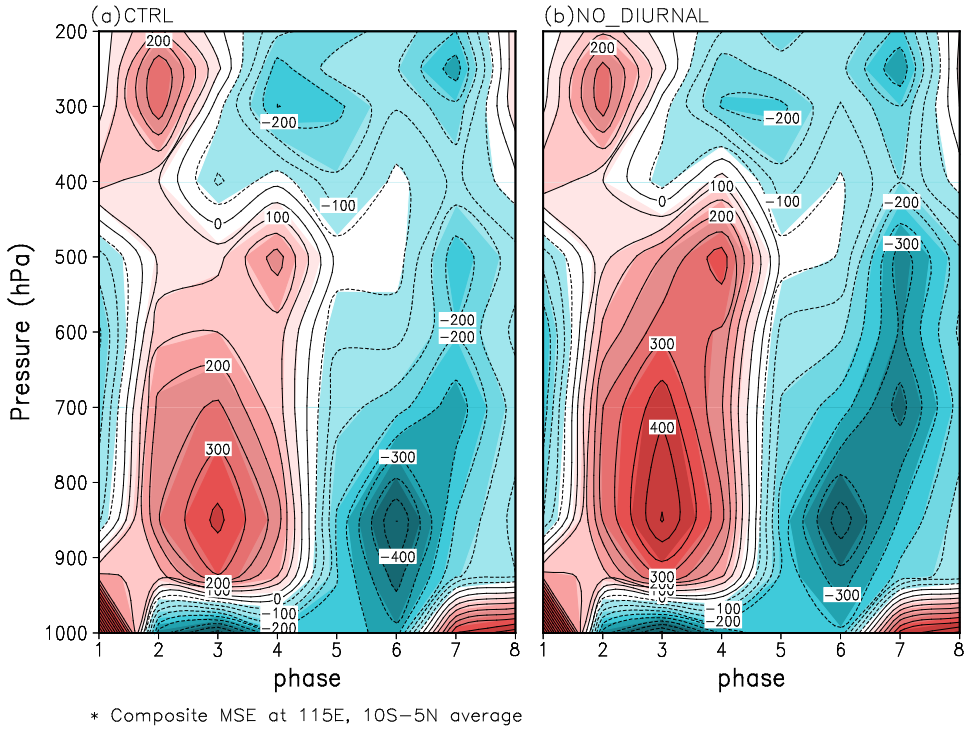

Figure 3.17 Composite equatorial (10°S–5°N averaged) intraseasonal moist static energy anomalies at 115°E from (a) CTRL and (b) NO_DIURNAL. The contour interval is 50 J/kg.

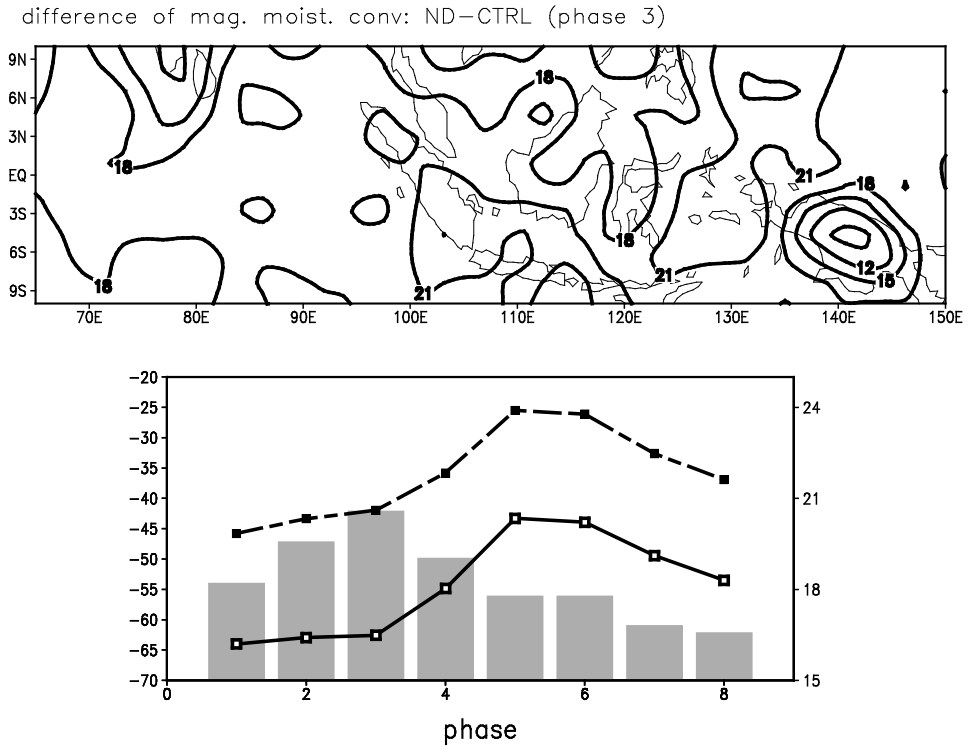

Figure 3.18 Composite of the daily mean convective instability difference between NO_DIURNAL and CTRL experiment at MJO phase 3 (top) and daily mean convective instability averaged over lat:10°S–5°N, lon:100°E-120°E (bottom) with respect to MJO phase. Dashed line represents CTRL and solid line represents NO_DIURNAL simulation. Y-axis on the left denotes the convective instability. Bar graph represents the difference of the convective instability between NO_DIURNAL and CTRL at each MJO phase.

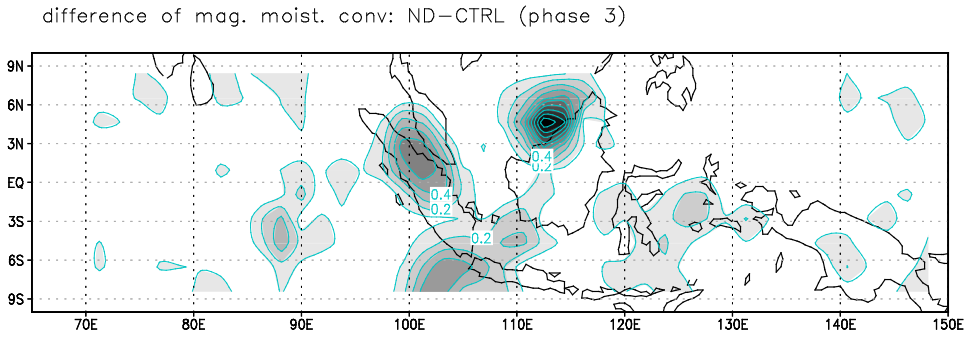

Figure 3.19 Composite of the daily mean moisture convergence at 850 hPa difference between NO_DIURNAL and CTRL experiment at MJO phase 3. (contour interval is 0.2 ×10-6 g/kg/sec)

Chapter 4

Summary and conclusion

We investigate the impact of MJO on the diurnal cycle of rainfall over the western Maritime Continent by applying CSEOF analysis to the TRMM rain rate andJRA-25 reanalysis data. The RMM index defined by Wheeler and Hendon (2004) is adopted to define the intensity and phase of MJO. Based on the PC time series of the diurnal cycle of rain rates, MJO with intraseasonal time scales is found to modulate the diurnal variation of rainfall over the analysis domain. In addition, during the active phases of MJO as defined by the RMM index, the average magnitude of the PC time series tends to increase indicating an enhancement of the diurnal cycle.

CSEOF analysis is also performed separately for each MJO phase as defined by the RMM index. We demonstrate that domain averaged hourly maximum rain rate tends to increasewhen the convectively active phase of MJO approaches and resides over the Maritime Continent (phase 3). In contrast,

when convectively inactive MJO phase is found over the region (phase 7), hourly maximum rain rate tends to subside. The magnitude of the diurnal cycle is larger in the morning than the magnitude of climatology, but is smaller in the evening during the mature phase (phase 5).The rain rate change due to MJO differs over the ocean and land. This discrepancy is most apparent during phase 5. While diurnally varying oceanic rain rates record maximum values, terrestrial rain rates show minimum values throughout the day during phase 5. Precipitation becomes more intense over the Java Sea in the morning and weakened over Borneo and Sumatra in the evening during phase 5.

The percentage of the oceanic region recording maximum rain rates at each local time is examined with respect to MJO phase. During the developing stage of MJO convection over the western Maritime Continent, the percentage is greatest at 0500 LST unlike the climatology andother phases, in which the percentage reaches its maximum at 0800 LST. Over land, in contrast, maximum rain rates are observed at 1700 LST regardless ofMJO phase. We hypothesize that the 3-hr advance of the maximum rain rates over

the oceans during phases 3 is tied to the combined effect of the physical process of the diurnal cycle of precipitation over the open ocean, which is not fully understood, and the initiation and propagation mechanisms of MJO. This combined effect leaded to favorable conditions for precipitation earlier over oceanic regions. However, this relationship requires further detailed examination.

Our results suggest that the anomalous low-level winds accompanied by MJO interact with the monsoonal flow over the Maritime Continent. Prevailing westerlies to the west of the convective MJO in phase 5 are superimposed on monsoonal westerlies over the equator and increase wind speed mainly over the Java Sea due to the blocking effect of orography. Mountainous islands induce flow bifurcation making near-surface winds prevail over the oceanic channels between two islands (Wu and Hsu, 2009). As a result, heat flux release from the oceans to the atmosphere is enhanced by the increased surface wind giving rise to instability as described in the wind-induced surface heat exchange (WISHE) mechanism (Emanuel 1987; Neelin et al. 1987). This may contribute to heavy rainfall over the Java Sea

in the morning during phase 5.

The presence of strong convergence at 925hPa in conjunction with an upward motion at 500 hPa over the Java Sea also explains strong rain rate in the morning during phase 5. On the other hand, evening convergence and vertical velocity over the islands tends to be weakerduring the mature phase (phase 5) than the developing or decaying phases (phases 3 or 7). Strong westerlies contributed by the anomalous wind accompanying MJO and seasonal flow during phase 5 tend to interrupt convergences over islands that play important roles in inducing nighttime rainfall. This interruption results in decreased rain rate over terrestrial regions compared to the phases 3 and 7. The existence of fully developed cloud clusters of MJO over the Maritime Continent may also contribute to decreased rain rate over the islands. As cloud clusters reside over the Maritime Continent during phase 5, they intercept daytime solar radiation, which results in decreasedpressure gradient between land and the ocean. Ultimately, the decreased pressure gradient leads to a decreased precipitation over land in the afternoon. This hypothesis should be examined further using cloud data.

We investigate the impact of MJO on the diurnal cycle of rainfall over the Maritime Continent, and attempted to explain the physical processes behind the land/ocean differential impacts of MJO on the diurnal variation of precipitation. Large regional variability is inherent in the diurnal cycle (Lim and Seo 2000) and it cannot be ruled out that inhomogeneous surface condition over the Maritime Continent is responsible for differential impact of MJO (Byon and Lim 2005). Moreover, dynamical link between the diurnal cycle and MJO competing for the limited source of moisture may involve multiple interactions of complicated physical mechanisms. Sophisticated analysis based on dense observations and numerical modeling is needed to answer these questions.

We use modeling experiments to investigate the impact of the diurnal cycle on the MJO during the Australian summer. Physical initialization and a nudging technique enable us to assimilate observed TRMM rain rate and atmospheric variables from the NCEP R2 into the FSUGSM, resulting in a realistic simulation of the basic climatology of rainfall during austral summer (DJF) and the MJO. We modulate the diurnal cycle from the model

integration by assimilating daily averaged fields of precipitation, surface pressure, temperature, vorticity, divergence, and specific humidity and examine the results. Globallyeliminating the diurnal cycle exerts a strong influence on the Maritime Continent. The mean state of precipitation increases and the intraseasonal variability becomes stronger over the region. Whereas the MJO isusually weakened when it passes over the Maritime Continent, it does maintain its strength in the NO_DIURNAL experiment. However, neglecting the diurnal signals during the integration does not change the propagating speed of the MJO.

As Inness and Slingo (2006) mentioned in their study, the enhanced diurnal cycle of convection may interfere with the relatively slow development of the MJO over the Maritime Continent by dissipating moist static energy on a rapid time scale. We demonstrate that stronger MSE buildup occurs before the MJO convection develops over the Maritime Continent in NO_DIURNAL in comparison to MSE buildup in CTRL. The result suggests that deliberately diminishing the diurnal cycle in the model experiment consumes less MSE, leaving more MSE for the MJO’s buildup,

an sufficient condition for the development of MJO convection in terms of the recharge–discharge theory of MJO. Along with the increased build up of MSE, composites of conditional instability and low-level moisture convergence provide supporting evidence for the amplification of the MJO in the experiment with a modulated diurnal cycle. With stronger moisture convergence under the conditional instability, the MJO tends to maintain its amplitude by using enough MSE over the Maritime Continent in the NO_DIURNAL experiment.

While the present study attempts to concentrate on the impact of the diurnal cycle on the MJO, previous studies emphasized the direct influence of the topography inweakening the MJO as it passes over the Maritime Continent. Hsu and Lee (2005) focused on the relationship between MJO deep convection and tropical topography. They suggested that the lifting and frictional effects of the tropical topography and landmasses of the Maritime Continent under the prevailing surface easterly anomalies of the MJO induce the near-surface moisture convergence anomaly, which in turn triggers the deep heating anomaly. As a result, a subsequent new heating

anomaly develops to the east of the topography. Meanwhile, the previous heating anomaly located to the west of the tropical topography weakens. Inness and Slingo (2006) investigated the blocking effect of the islands of the Maritime Continent using a simplified, aqua-planet version of GCM, with various idealized configurations of the Maritime Continent. They suggested the orography of the islands, rather than the presence of the islands themselves, as the main reason for the reduction in strength of the MJO as it passes over the Maritime Continent. Wu and Hsu (2009) addressed the blocking and wave-making effect of the topography on the MJO over the Maritime Continent. They found that the eastward movement of deep convection and near-surface wind anomalies in the MJO skirt the islands, resulting in a southward detour of the eastward-propagating MJO and a sudden shift of deep convection from one region to another. In addition, extra lifting and sinking within the large-scale circulation are induced by thetopography, therefore modifying the behavior of the MJO in the Maritime Continent.

We do not rule out either the blocking effect of the islands or the influence

of orography in the weakening of the MJO over the Maritime Continent. The existence of land–sea contrast over the region does trigger the diurnal cycle. However, the diurnal cycle itself may play a major role in controlling MJO intensity over the Maritime Continent. The continuing debate over theories regarding the MJO necessitates further investigation using high-resolution model with a more sophisticated land scheme.

References

Back L,Bretherton C (2006) Geographic variability in the export of moist static energy and vertical motion profiles in the tropical Pacific.Geophys Res Lett 33: L17810, doi:10.1029/2006GL026672.

Bowman K, Collier J, North G, Wu Q, Ha E, Hardin J (2005) Diurnal cycle of tropical precipitation in Tropical Rainfall Measuring Mission (TRMM) satellite and ocean buoy rain gauge data. J Geophys Res doi:10.1029/2005JD005763

BladéI, Hartmann D(1993) Tropical intraseasonal oscillations in a simple nonlinear model. J AtmosSci 50:2922-2939

Bloom, S, Takacs L, Brin E (1996) Data assimilation using incremental analysis updates.Mon Wea Rev 124:1256-1271

Byon J, Lim G (2005) Diurnal variation of tropical convection during TOGA COARE IOP. AdvAtmosSci 22:685-702

Cane M, Molnar P (2001) Closing of the Indonesian seaway as a precursor to east African aridification around 3–4 million years ago *Nature411:*157–162.

Chen S, Houze JrR (1997) Diurnal variation and life-cycle of deep convective systems over the tropical Pacific warm poolQ J R Meteorol Soc 123(538):357-388

Cocke S,LaRow T (2000) Seasonal prediction using a regional spectral model embedded within a coupled ocean atmosphere model. Mon Wea Rev 128:689-708

Dayem K, Noone D, Molnar P (2007) Tropical western Pacific warm pool and maritime continent precipitation rates and their contrasting relationships with the Walker Circulation. J Geophys Res 112:doi:10.1029/2006JD007870

Emanuel K (1987) An air-sea interaction model of intraseasonal oscillations in the tropics. J AtmosSci 44:2324-2340

Gill A (1980) Some simple solutions for heat induced tropical circulation.Q J R Meteorol Soc 106(449):447-462

Gray W, Jacobson Jr R (1977) Diurnal variation of deep cumulus convection. Mon Wea Rev 105:1171-1188

Hall J, Matthews A, Karoly D (2001) The modulation of tropical cyclone

activity in the Australian region by the Madden-Julian oscillation. 87 Mon Wea Rev 129:2970-2982

Held I, Cook K, (1987) Evaporation-wind feedback and low-frequency variability in the tropical atmosphere. J AtmosSci 44:2341-2348

Hendon H, Liebmann B (1990) The Intraseasonal (30-50 day) Oscillation of the Australian Summer Monsoon. J AtmosSci 47:2909-2924

Hendon H, Salby M, (1994) The life cycle of the Madden-Julian oscillation. J AtmosSci 51:2225-2237

HouzeJr R, Geotis S, Marks Jr F, West A (1981) Winter monsoon convection in the vicinity of North Borneo. Part I: Structure and time variation of the clouds and precipitation. Mon Wea Rev 109:1595-1614

Hsu H, Lee M (2005) Topographic effects on the eastward propagation and initiation of the Madden-Julian oscillation. J Clim 18:795-809

Huffman G, Adler R, Arkin P, Chang A, Ferraro R, Gruber A, Janowiak J, McNab A, Rudolf B, Schneider U (1997) The global precipitation climatology project (GPCP) combined precipitation dataset. Bull Am Meteorol Soc 78(1):5-20

Ichikawa H, Yasunari T (2006) Time-space characteristics of diurnal rainfall over Borneo and surrounding oceans as observed by TRMM-PR. J Clim 19:1238-1260

Ichikawa H, Yasunari T (2007) Propagating diurnal disturbances embedded in the Madden-Julian Oscillation. Geophys Res Lett 34:doi:10.1029/2007GL030480

Inness, P. M., and J. M. Slingo (2006), The interaction of the Madden-Julian oscillation with the maritime continent in a GCM, *Quarterly Journal of the Royal Meteorological Society*, *132*(618), 1645-1667.

Johnson R, Kriete D (1982) Thermodynamic and Circulation Characteristics, of Winter Monsoon Tropical Mesoscale Convection. Mon Wea Rev 110:1898-1911

Kemball-CookS, Weare B (2001) The onset of convection in the Madden–Julian Oscillation. JClim14:780–793

Kemball-Cook S, Wang B, Fu X (2002) Simulation of the intraseasonal oscillation in the ECHAM-4 model: The impact ofcoupling with an ocean model. JAtmos Sci 59: 1433-1453

Kessler W, Kleeman R (2000) Rectification of the Madden-Julian oscillation into the ENSO cycle. J Clim 13:3560-3575

Kikuchi K, Wang B (2008) Diurnal precipitation regimes in the global tropics*. JClim21:2680–2696

Kim, D., K. Sperber, W. Stern, D. Waliser, I. S. Kang, E. Maloney, W. Wang, K. Weickmann, J. Benedict, and M. Khairoutdinov (2009), Application of MJO simulation diagnostics to climate models, J Clim, *22*(23), 6413-6436.

Kim K, North G (1997) EOFs of harmonizablecyclostationary processes. J AtmosSci 54:2416-2427

Kim K, North G, Huang J (1996) EOFs of one-dimensional cyclostationary`time series: Computations, examples, and stochastic modeling. J AtmosSci 53:1007-1017

Kraus E (1963) The diurnal precipitation change over the sea. AtmosSci 20:546-551

Krishnamurti T, Xue J, Bedi H, Ingles K, Oosterhof D (1991) Physical initialization for numerical weather prediction over the tropics.

Tellus 43AB:53-81

Krishnamurti T, Rohaly G, Bedi H (1994)On the improvemnet of precipitation forecast skill from physical initialization. Tellus 46A:53-81Lim G, Suh A (2000) Diurnal and semidiurnal variations in the time series of 3-hourly assimilated precipitation by NASA GEOS-1.JClim, 13(16), 2923-2940

Lawrence D, Webster P (2002) The boreal summer intraseasonal oscillation: Relationship between northward and eastward movement of convection. J AtmosSci 59:1593-1606

Liberti G, Cheruy F, Desbois M (2001) Land effect on the diurnal cycle of clouds over the TOGA COARE area, as observed from GMS IR data. Mon Wea Rev 129:1500-1517

Lim G, Seo A (2000) Diurnal and semidiurnal variations in the time series of 3-hourly assimilated precipitation by NASA GEOS-1. J Clim 16:2923-2940

Madden R, Julian P (1994) Observations of the 40 50-day tropical oscillation A review.Mon Wea Rev 122(5):814-837

Maloney E (2009) The moist static energy budget of a composite tropical intraseasonal oscillation in a climate model. JClim22:711–729

Maloney E, Hartmann D (2000) Modulation of eastern North Pacific hurricanes by the Madden-Julian oscillation. J Clim 13:1451-1460

Matsumoto J (1992) The seasonal changes in Asian and Australian monsoon regions. J Meteor Soc Japan 70:257–273 90

Mori S, Jun-Ichi H, Tauhid Y, Yamanaka M, Okamoto N, Murata F, Sakurai N, Hashiguchi H, Sribimawati T (2004) Diurnal Land-Sea Rainfall Peak Migration over Sumatera Island, Indonesian Maritime Continent, Observed by TRMM Satellite and Intensive Rawinsonde Soundings. Mon Wea Rev 132:2021-2039

Neale R, Slingo J (2003) The maritime continent and its role in the global climate: A GCM study.JClim 16(5):834-848

Nesbitt S, Zipser E (2003) The diurnal cycle of rainfall and convective intensity according to three years of TRMM measurements. J Clim 16:1456-1475

Nunes A, Cocke S (2004) Implementing a physical initialization procedure

in a regional spectral model: impact on the short-range rainfall forecasting over South America. Tellus A56:2, 125-140

Onogi, K., J. Tsutsui, H. Koide, M. Sakamoto, S. Kobayashi, H. Hatsushika, T. Matsumoto, N. Yamazaki, H. Kamahori, K. Takahashi, S. Kadokura, K. Wada, K. Kato, R. Oyama, T. Ose, N. Mannoji and R. Taira, (2007) The JRA-25 Reanalysis. J Meteor Soc Japan 85:369-432

Qian J (2008) Why precipitation is mostly concentrated over islands in the Maritime Continent. J AtmosSci 65:1428-1441

Ramage C (1971) Monsoon Meteorology. Academic Press, 295 pp

Rauniyar P, Walsh K (2011) Scale interaction of the diurnal cycle of rainfall over the Maritime Continent and Australia: influence of the MJO. JClim24:325–348.

Rui H, Wang B (1990) Development characteristics and dynamic structure of tropical intraseasonal convection anomalies. J AtmosSci 47:357-91

Salby M, Hendon H (1994) Intraseasonal behavior of clouds, temperature,

and motion in the Tropics. J Atmos Sci 51: 2207–2224

Sato T, Kimura F (2005) Diurnal Cycle of Convective Instability around the Central Mountains in Japan during the Warm Season.J Atmos Sci 62: 1626–1636

Seo K, Schemm J, Wang W, Kumar A (2007) The boreal summer intraseasonal oscillation simulated in the NCEP Climate Forecast System: The effect of sea surface temperature. Mon Wea Rev 135:1807-1827

Slingo J, Inness P, Neale R, Woolnough S, Yang G (2003) Scale interactions on diurnal to seasonal timescales and their relevance to model systematic errors. Ann Geophys 46:139-155

Slingo J, Sperber K, Boyle J, Ceron J, Dix M, Dugas B, Ebisuzaki W, Fyfe J, Gregory D, Gueremy J (1996) Intraseasonal oscillations in 15 atmospheric general circulation models: results from an AMIP diagnostic subproject. ClimDyn 12:325-357

Sperber K (2003) Propagation and the vertical structure of the Madden-Julian oscillation. Mon Wea Rev 131:3018-3037

Sui C, Lau K (1992) Multiscale phenomena in the tropical atmosphere over the western Pacific. Mon Wea Rev 120:407-430

Sui C, Lau K, Takayabu Y, and Short D (1997) Diurnal variations in tropical oceanic cumulus convection during TOGA COARE. J AtmosSci 54:639-655

Tian B, Waliser D, Fetzer E (2006) Modulation of the diurnal cycle of tropical deep convective clouds by the MJO. Geophys Res Lett 33:doi:10.1029/2006GL027752

Wheeler M, Hendon H (2004) An all-season real-time multivariate MJO index: Development of an index for monitoring and prediction. Mon Wea Rev 132:1917-1932

Wu C, Hsu H (2009) Topographic Influence on the MJO in the Maritime Continent. J Clim 22:5433-5448

Yang G, Slingo J (2001) The diurnal cycle in the Tropics. Mon Wea Rev 129:784-801

Yang S, Smith E (2006) Mechanisms for diurnal variability of global tropical rainfall observed from TRMM. J Clim 19:5190-5226

Zhang C, Gottschalck J (2002) SST Anomalies of ENSO and the Madden-Julian Oscillation in the Equatorial Pacific. J Clim 15:2429-2445

Zhou L, Wang Y (2006) Tropical Rainfall Measuring Mission observation 93

and regional model study of precipitation diurnal cycle in the New Guinean region. J Geophys Res 111:doi:10.1029/2006JD007243

국문초록

본 논문에서는 북반구겨울철에 Maritime Continent 상에서 일어나는 계절내 진동과 일변동 성분간의 상호작용을 연구하는 것을 목적으로 한다.

논문의 전반부에서는 북반구 겨울철에 MJO가 Maritime Continent 서쪽에서 강수의 일주기에 미치는 영향에 관하여 논하였다. 이를 위하여 1998년에서 2008년 사이의 TRMM 관측 강수율과 JRA-25 재분석자료에 Cyclostationary Empirical Orthogonal Function (이하CSEOF) 분석방법을 적용하였다. Wheeler와 Hendon이 2004년에 고안한 RMM 지수를 채택하여 MJO의 위상과 강도를 정의하였다. 이 결과, 대류적으로 활발한 MJO가 Maritime Continent에 접근할 때, 분석 영역에서 시간당 내리는 강수량이 증가하는 것이 확인되었다. 반대로 대류적으로 쇠퇴한 MJO가 분석영역에 머무를 때는 강수율이 감소하는 양상을 보였다. 해양에서의 MJO에 의한 강수율의 변화는 대륙에서의 변화와 차이가 나는 것으로 드러났다. Maritime Continent 상에서

MJO의 최성기에 육지의 강수율은 하루 종일 계절 평균 값을 밑도는 반면에, 해양에서의 강수율의 일주기 성분은 평균 값보다 증가하는 것이 밝혀졌다. 즉, MJO의 최성기에 Java 해에서 오전 강수는 강화되는 반면, 저녁시간의 Borneo와 Sumatra의 강수는 감소하였다. MJO의 쇠퇴기에는 대륙과 해양 모두 강수량이 줄어 들지만, 그 감소폭이 대륙에서 더 컸다.

분석결과, MJO가 동반하는 하층의 바람장이 Maritime Continent 상의 몬순에 의한 계절풍과 상호작용함으로 인하여 위와 같은 결과를 발생 시키는 것이 드러났다. MJO 최성기에 이로 인해 발생하는 서풍은 몬순에 의한 서풍에 중첩되어 Maritime Continent 상의 풍속 증가를 야기시킨다. 이렇게 증가한 기류는 이 지역의 산악지형 때문에 흐름을 방해 받게 됨으로써 상대적으로 마찰이 작은 Java 해 상에서 풍속의 증가가 더욱 두드러지게 된다. 이지역의 기류는 산악지형을 피해 해상으로 우회함으로 섬들 사이의 좁은 해양 상공으로 기류가 수렴하게 된다. 그 결과, 해수면 표면에서의 풍속이 증가하게 되면서 대기가 불안정하게 되고, 결국 해양으로부터 대기 중으로 열속 (heat flux)이 방출된다. 이러한 과정을 통

하여 MJO 최성기에 Java 해에서 오전 강수량이 증가하는 것으로 추정된다. 반면에 내륙지역의 야간 강수를 일으키는데 중요한 역할을 하는 육지상의 대기의 수렴과 상승운동은 MJO의 최성기에 그 활동이 약화됨이 보여졌다. MJO로부터 유발된 하층서풍과 Maritime Continent에서의 계절풍이 중첩되면서 내륙지역의 기류의 수렴을 동쪽으로 밀어내게 된다. 이처럼 수렴 활동이 방해를 받게 되면서 내륙지역의 야간강수가 감소하게 되는 것으로 추정된다.

본 연구의 후반부에서는 수치 모델실험을 통하여 북반구 겨울철에 일변동 성분이 계절내 진동 현상에 미치는 영향에 관하여 논하였다. 물리적 초기화와 너징 (nudging) 기법을 이용하여 NCEP R2 재분석자료와 TRMM 관측 강수율을 플로리다 주립대학 스펙트럴 모델에 동화할 수 있다. 이러한 과정을 통해 재현된 MJO는 관측과 상당히 유사한 형태를 보인다. 이러한 자료 동화 기법을 응용하여 일변동 성분을 개조한 후, 이렇게 변형된 일변동 현상이 MJO 모의에 어떠한 영향을 미치는가를 알아보았다. 하루를 주기로 변하는 성분 대신에 일평균된 값을 동화해 줌으

로써 모델내 일주기 성분의 강도를 약화시켰다. 전구영역에 걸쳐 감소된 일변동 성분은 특히 Maritime Continent 상에 강한 영향을 미치는 것으로 확인되었다. 이 지역의 평균 강수뿐만 아니라 계절내 진동성분의 강도도 증가하였다. 선행 연구를 통하여 MJO가 Maritime Continent를 통과할 때, 그 활동이 약화되는 것이 밝혀졌으나 본 연구에서 수행된 모델 실험에서는 이러한 MJO의 강도가 유지되는 것이 밝혀졌다. 일변동 성분의 약화는 강수 일변동과 MJO의 발생에 모두 필요한 습윤정적 에너지의 소모를 줄이게 되고, 이렇게 남아도는 습윤정적 에너지는 강한 대류불안정과 하층의 수분 수렴과 함께 Maritime Continent 상에서의 MJO의 진폭을 유지시키는 것으로 추정된다.

주요어: 계절내진동, 일변동성분, 규모상호작용, 물리적초기화

학번: 2007-30103